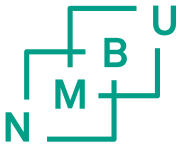
U
B
M
N

Norwegian University of Life Sciences

Faculty of Environmental Sciences and Technology

Department of Mathematical Sciences and Technology

Terrestrial Gravimetry for Cryospheric Mass Variations

Observations and Modelling at Svartisen Glacier, Norway

Author:
Siri Eikerol

Supervisors:
Christian Gerlach
Jon Glenn Gjevestad
Bjørn Ragnvald Pettersen

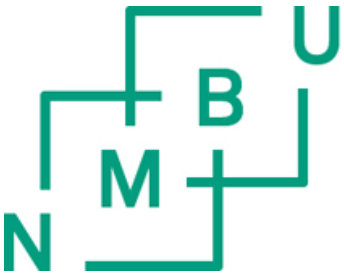

June 20, 2014

Abstract

Glacier ice stores about 75 % of the worlds freshwater, a basic resource for life, and a primary medium through which climate change affects the Earth's ecosystem and its habitants. Glaciers are sensitive climate change indicators, and in Norway research on glacier mass balance is of interest e.g. in the scientific field of glaciology as well as for hydro power production companies.

This thesis presents a method for observing mass change of glacier ice on Engabreen drainage basin, a part of Western Svartisen ice cap, Norway. The Norwegian Water Resources and Energy Directorate operates a subglacial laboratory situated below 200 m of ice. The laboratory area is a part of a long system of water tunnels leading melt water from the glacier bed to hydro power production. The site gives opportunities for measuring very precise gravity values in laboratory conditions with an absolute gravimeter. Relative gravity measurements were conducted in the water tunnel leading from one side of the glacier outlet tongue to the other.

Field work was conducted during March 2014 in order to establish gravity stations for facilitating later missions and develop a time series for the given conditions. Twenty one gravity stations were surveyed and marked through the specified part of the tunnel system. An absolute gravity value of 982202709.74 μGal with an uncertainty of $\pm$ 3.47 μGal was measured at the laboratory site and the relative measurements showed uncertainties of around 10 μgal. Modelled effects of different ice surface changes, and the uncertainties of the gravity measurements, give an opportunity to detect changes of $\pm$ 0.05 m on the glacier surface.

Temporal masses in the tunnel system were measured during the field work and the effect on nearby gravity stations was modelled. For forthcoming missions, these effects can be reduced if other conditions occur. The present work describes a method for determining a more precise bedrock topography, which may give more accurate results of the gravity effects.

With the results presented additional data can be combined with established methods for mass measurements and give more precise results in interest of hydro power production and for scientific purposes related to climatic change.

Samandrag

Omlag 75% av alt ferskvatn på jorda er bunde i is og isbrear. Ferskvatn er ein ressurs som er naudsynt for alt liv, men er og ei kjelde til at økosystem og folk vert påverka av klimaendringar. Isbrear er sensitive med omsyn til klimaendringar, og forsking på masseendring av isbre er av interesse både i høve til glasiologi og vasskraftproduksjon.

Denne masteroppgåva presenterer ein metode for å observere masseendringar i isbre. Det er gjennomført observasjonar ved Engabreen, som er ein brearm av Svartisen i Nordland. I tilknytning til Engabreen er det etablert eit tunnelsystem som leier smeltevatn frå breen til bruk i vasskraftproduksjon. Noregs vassdrag- og energidirektorat driftar eit laboratorium i tilknytning til dette tunnelsystemet som ligg under 200 m is. Fasilitetane gjer det mogleg å gjere målingar under laboratorietilhøve med eit absolutt gravimeter, og det er utført relative tyngdemålingar i tunneldelen som går under brearmen.

Feltarbeiet vart gjennomført i mars 2014. Det vart etablert eit nettverk av tyngdestasjonar for å kunne gjere observasjonar ved eit seinare tidpunkt og samstundes etablere ein tidsserie av tyngdemålingar. Tjueein tyngdestasjonar vart oppmålt og merka med bolt gjennom tunnelsystemet. Den absolutte tyngdeverdien i laboratoriet vart målt til 982202709.74 $\pm$ 3.47 μGal, og det vart knytt relative målingar til denne. Dei relative målingane viser usikkerheit på omlag 10 μGal. Med denne usikkerheita kan ein detektere endring p overflata av isbreen på $\pm$ 0.05 m i tyngdeobservasjonane.

Det er målt tidsvarierande massar i tunnellen, og effektar av desse er estimert på tyngdestasjonane for å utelukke avvik i seinare arbeid. Kombinert med etablerte metodar for å måle masseendringar, kan ein få meir presise resultat, noko som kan vere av interesse for vasskraftproduksjon og for til dømes glasiologi. Oppgåva presenterer ein metode for å bestemme overgangen mellom fjell og is under breen meir presist enn det som idag er tilgjengeleg.

Acknowledgements

I would like to thank my supervisors for leading me through this process. I especially thank Christian Gerlach for letting me join the circus and giving me an exceptional opportunity to live in a tunnel. Organizing the field work and driving the equipment all the way from Munich to Holandsfjorden and back, after a week of 12-hour days, he has shown me many different aspects of scientific work. Jon Glenn Gjevestad has offered tireless patience when training with instruments at the university campus in Ås, and as a direct help line from Svartisen to Ås when everything seemed like it had gone all wrong. Bjørn Ragnvald Pettersen has been a good help in processing and understanding the raw data from the absolute gravity readings and given endless motivational and thematic speeches in his office.

Without the crew coming with to the field work at Svartisen, this thesis would not have been possible, and I give Alexander Helland and Vegard Ophaug a special thank for coming along and use their time and energy to get the work done.

Miriam Jackson at NVE deserves thanks for introducing me to this project, for guidance through the tunnel system and good help before, during and after the mission. I would also like to thank NVE and Hallgeir Elvehøy for providing data for the site.

My parents: thank you for support and interest in my work.

Finally I would like to thank my best friend and partner Fredrik for playing the double bass.

Contents

List of Figures

List of Tables

1 — Introduction

The statistical fields of freshwater can be filtered into several different topics. UN Water Agency[1] presents some of their topics as development, urbanization, water quality, climate change, water security and water and food. In their thematic fact sheets it is stated that water is the primary medium through which climate change affects the Earth's ecosystem and its habitants. Water is however, one of the basic resources of life with 70 % of the water withdrawals connected to agriculture and food production. For future insight, the UN states that by 2025, 1.8 billion people will be living in countries or regions with absolute water scarcity (UN, 2014).

In total, glacier ice stores about 75 % of the total amount of the freshwater (NSIDC, 2014), and almost 16 million km^2 of the Earth's surface is covered by glacier ice. About 500 000 km^2 exist as glaciers as well as ice caps and ice sheets. The latter two can be described as ice which is not constrained by the topography of the underlying bedrock. Antarctica and Greenland have the greater areas of this type. Glaciers are defined as ice that is constrained by the underlying topography (Benn and Evans, 2010).

Glacier ice is mainly influenced by the position in high mountains and at high latitudes. At higher latitudes, the solar angle will be lower and therefore gives less solar energy to heat the surface, and it affects the temperature as the air is less dense. Also, the distance to a moisture source will affect the position of glacier ice (Liestøl, 2000). As well as contributing to the fresh water supply to rivers and local hydrology in glacierized regions, water released from glaciers can cause serious hazards of flooding and damage to infrastructure with major consequences to human life (Benn and Evans, 2010).

Norway, having more than 2500 glaciers covering over 2600 km^2 of the land area (Andreassen et al., 2012), has a unique possibility to survey and extract resources from glaciers. Hydropower production in Norway has a capacity of producing over 130 TWh a year (NVE, 2014c), and glaciers influence the rivers and basins discharge and have thus resulted in extensive measurements of the glaciers. As glaciers are sensitive climate change indicators, climate research including mapping of glacier outlines is of interest. Systematic observations of glaciers in Norway started around 1900 with glacier length measurements, and some of these series are continuous to the present day (Andreassen et al., 2012).

[1] *The United Nations inter-agency mechanism on all freshwater related issues, including sanitation*

1.1 Svartisen Subglacial Laboratory

In 1989, the Norwegian Water Resources and Energy Directorate (NVE), together with Statkraft, started the construction of subglacial water intakes beneath one of Western Svartisen ice caps outlets glacier, Engabreen (Fig. 1.1). Statkraft is a state-owned power producer with an annual power production of 56 TWh, and of these 97 % is renewable energy (*statkraft.no*). The hydro-electrical power plant connected to the subglacial water intakes, Svartisen Kraftverk, has an annual power production of 2170 GWh (vasskraft.no, 2014).

Western Svartisen ice cap is situated in northern Norway, between $66^o33'$ - $66^o47'$ N, and $13^o40'$ - $14^o8'$ E, just north of the Artic Circle. The ice cap covers an area of 221 km^2 and is the second largest glacier in Norway (SNL, 2014). Engabreen outlet glacier is heading northwest towards Holandsfjorden, only separated by the lake, Engabrevatnet.

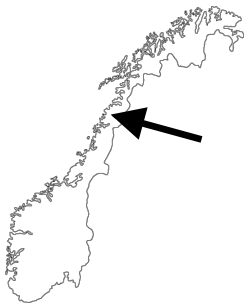

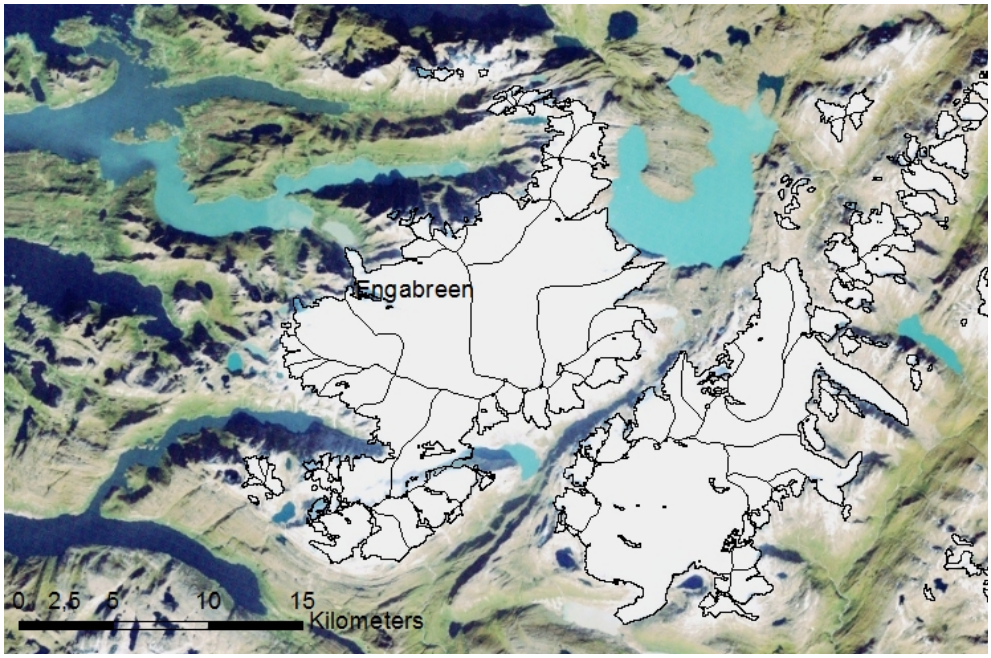

Figure 1.1: Map over Svartisen ice cap and the separate drainage basins

The tunnel entrance leading to the laboratory lies at 512 m above sea level and can be accessed by foot or by helicopter. From the entrance, a stunning view can be experienced over Engabreen outlet glacier; the steep mountains characteristic of the region and the North Sea. About 1500 m into the tunnel, a subglacial laboratory is built with access to the glacier bed through a dedicated tunnel shaft. The ice is about 200 m thick at this position (NVE, 2014b). An all-facilities housing quarter is built

closer to the tunnel entrance which facilitates research projects for longer time periods (fig. 1.2).

Figure 1.2: Laboratory housing

1.2 Aim of study

With this study, the establishment of gravity stations beneath Engabreen drainage basin, for ongoing time series of gravity measurements has the potential to provide valuable data to the research of mass balance studies at the site. Measuring with an absolute gravimeter will give a gravity value of high precision and with measurements from relative gravimeter gravity values with high precision can be obtained throughout the tunnel. Modelling of temporal mass changes that can affect the measurements will be done subsequently.

With error analysis of the gravity values defined for the stations, a final range of detectable changes in glacier mass and other temporal mass distributions can be derived from surface models. The gravity measurements will be carried out with an absolute gravimeter and relative gravimeters.

The work will be carried out as a master study at the Norwegian University of Life Sciences (NMBU).

2 — Glaciers and glacier mass balance

The solid form of water on the Earth's surface comprises the *cryosphere*. The Greek word expressing cold, *kryos*, has given name to this part of the Earth's system. Sea ice, lake ice, snow cover together with glaciers and ice sheets all belong to the *cryosphere*, which overlaps with the *hydrosphere* as the climatic conditions change over seasons. Glaciers are perennial bodies and as the rest of the *cryosphere*, they are sensitive to climate change. As a response to e.g. temperature change and precipitation, the glaciers are in constant change, displayed as growing or shrinking of the ice masses, which can be measured in different ways (Benn and Evans, 2010).

Along with the freezing temperature of water, glaciers are found in areas where the climatic conditions allow the mass balance to hold equilibrium state or where the ablation (mass loss) is less than the accumulation (mass gain). Areas with such cold conditions are found mainly in higher mountainous areas or at high latitudes. These properties lead to an abundance of snow and ice during the year, and the glacier will increase or decrease relative to the surrounding conditions (Liestøl, 2000). This chapter will give a short introduction to the physics of ice and short presentations of methods for determining the mass balance of a glacier.

The physics of glaciers

A glacier is essentially snow packed to the density of ice, however, glacier ice has properties differing from pure ice (Table 2.1).

Table 2.1: Physical constants of glacial ice

Density	
Pure ice	$\rho = 917 kg/m^3$
Glacier ice	$\rho = 900 kg/m^3$
Melting point	
1 atm [2]	$0^o C$

2.1 Observational methods

Mass balance of glaciers is a well established measurement and refers to the volume change of the ice during a season or defined time period. It relates to the accumulation or ablation of ice and snow on the glacier. The mass balance can be calculated for the whole glacier or for specific areas, and the time period is often a calender year or balance year (interval between two successive annual minima). The mean specific mass balance, also called the area-averaged mass balance, is the total change in mass divided by the area of the glacier (Benn and Evans, 2010). Three methods are described.

2.1.1 Glaciological method

Measurements are done directly in the glacier surface by using stakes drilled into the ice and the amount of snow and/or ice lying on top of the ice is related to a reference surface (eg. previous summer surface). As more precipitation occurs, this affects the snow below with considerable weight and the density along the vertical direction changes. Samples of the accumulated mass are taken to find the water equivalent. The net annual accumulation, b_a, is expressed in terms of water equivalent in equation 2.1,

$$b_a = h(\frac{\rho_i}{\rho_w}) \tag{2.1}$$

where h is the thickness of the annual layer, ρ_i is the average density of the layer and ρ_w is the water density (Benn and Evans, 2010). The total mass balance of a glacier surface is interpolated from the sampling points or calculated as a function of elevation (Kaser et al., 2003).

2.1.2 Geodetic method

By using surface elevation models, the mass balance can be estimated by the change of elevation between two different surface models made at two different dates (Kaser et al., 2003). Estimates of the surface density converts the surface differences into mass change, but uncertainties in these estimates put limitations to this method as the volume change may vary compared to the change in mass. Surface models can be derived from aerial photography or satellite data, and then makes it possible to calculate the mass balance of glacier ice in poorly accessible areas and of continent-scale ice sheets. Dynamic changes and calving can also be detected by the geodetic method (Benn and Evans, 2010).

[2]With increasing pressure, the melting point, also referred to as the pressure melting point, drops with 0.0073^{o}C/bar (Liestøl, 2000).

2.1.3 Gravimetric method

With satellite gravimetry, changes in the Earth's mass distribution can be directly measured. In contrast to the glaciological and geodetic methods, the gravimetric method directly detects the change in mass, rather than the change in volume. Large areas can be covered and integrated over, and thus signals from other mass redistributions, e.g. isostatic rebounds, must be separated (Benn and Evans, 2010). Terrestrial gravimetry has a finer spatial resolution compared to satellite gravimetry, e.g. the dedicated space mission *Gravity Recovery and Climate Experiment* which observes signal from Earth's gravity field with a ground footprint of radius of 500 - 700 km (Breili and Rolstad, 2009).

Direct gravimetric measurements can be used as a technique to determine the thickness of glacier ice alone or together with seismic measurements, and from this deduce the total volume of the glacier. The accuracies achieved with this method depend on the validity of the regional gravity field as well as the density of the bed rock (Klingele and Kahle, 1977). As the strong gravitational gradient of the Earth influences terrestrial gravimetric measurements, the measurements are very sensitive to heights. Height changes on the glacier surface can be detected by this method as well as detection of changes in internal density caused by refreezing of melt water (Breili and Rolstad, 2009).

2.2 Mass balance of Svartisen/Engabreen

NVE has performed mass balance measurements at Engabreen annually since 1970. The mean net balance is +0.6 m water equivalent and an average snow depth on the glacier plateau of 6-8 m. Every year 10 -15 m of ice melts at the glacier tongue. The glacier dynamics, that is the movements of the glacier, have also been subject to measurements, and have revealed velocities up to 1.3 m per day close to the ice fall (NVE, 2014a). The geodetic mass balance of Western Svartisen ice cap for the time period 1968-1985 and 1985-2002 was described by Haug et al. (2009), based on a Master thesis at NMBU. Photogrammetric methods were used to obtain stereo images and derive digital terrain models for the years 1968, 1985 and 2002. The research concluded with a negative mass balance for Engabreen, the opposite of what NVE is operating with.

3 — Gravity field and gravimetry

Newton's law of gravitation states that any two point masses in a distance from each other will affect each other with an attractive force, called the gravitational force. On the surface of Earth any point masses will be affected by a gravitational force and, due to the rotation of the Earth, a centrifugal force. The resultant of these two forces is called gravity (Hofmann-Wellenhof and Moritz, 2006). This chapter will look more closely into the Earth's gravity field and describe methods for measuring gravity.

3.1 The gravity field

The gravitational force $\boldsymbol{F}$ (eq. 3.1) is defined by the gravitational constant G, the attracting body of mass m_1, the attracted body of mass m_2 and the distance between the two masses l,

$$\mathbf{F} = G\frac{m_1 m_2}{l^2}. \tag{3.1}$$

The gravitational constant was defined by Newton, and has the value

$$G = 6.6742 \cdot 10^{-11} m^3 kg^{-1} s^{-2}.$$

The attracting and the attracted masses, m_1 and m_2, attract each other completely symmetrically. For simplicity, equation 3.1 is applied on a unit mass,

$$\mathbf{F} = G\frac{m}{l^2}. \tag{3.2}$$

Equation 3.2 expresses the gravitational attraction exerted by the mass m on a unit mass at position P in a distance l from m.

The Earth's gravitational field is known as a conservative field, which means that the vector force field can be found as a scalar field,

$$V = G\frac{m}{l}, \tag{3.3}$$

where V, *the potential of gravitation*, is the potential of $\boldsymbol{F}$. Thus, the force vector is the gradient vector of the scalar function V (Hofmann-Wellenhof and Moritz, 2006). The components (in cartesian coordinates) of the gravitational field can be written

$$\mathbf{F} = [X, Y, Z] = gradV = \nabla V, \tag{3.4}$$

where

$$X = \frac{\partial V}{\partial x}, Y = \frac{\partial V}{\partial y}, Z = \frac{\partial V}{\partial z}. \tag{3.5}$$

If a continuous mass distribution in the Earth is assumed, the principle of the superposition holds and the total attraction of the Earth can be defined as the total potential of Earth given an estimate of the density ρ and the volume dv

$$V = G\int\int\int \frac{1}{r}\rho dv. \tag{3.6}$$

The centrifugal force f on a unit mass

$$f = \omega^2 p \tag{3.7}$$

is given by the angular velocity of the rotation of Earth ω and the distance from the axis of rotation p. As the attracting force, the centrifugal force can also be derived from a potential

$$\Phi = \frac{1}{2}\omega^2(x^2 + y^2). \tag{3.8}$$

The gravity is the resultant of two forces, gravitational and centrifugal, and the gravity potential W (eq. 3.9) is given by the resultant of the potential of the two forces; the potential of the gravitational force V and the potential of the centrifugal force Φ (Hofmann-Wellenhof and Moritz, 2006).

$$W = V + \Phi = G\int\int\int \frac{1}{r}\rho dv + \frac{1}{2}\omega^2(x^2 + y^2). \tag{3.9}$$

The gravity vector $\boldsymbol{g}$ (eq. 3.10), is denoted as the gradient vector of the potential W and has the physical dimensions of an acceleration (Hofmann-Wellenhof and Moritz, 2006).

$$\mathbf{g} = grad\, W = \left[\frac{\partial W}{\partial x}, \frac{\partial W}{\partial y}, \frac{\partial W}{\partial z}\right] \tag{3.10}$$

3.2 Level surfaces and plumb lines

At any point on the surface of Earth, a spirit level will coincide with an equipotential surface. This surface needs not be parallel with the surface of Earth as it is, unlike the surface of Earth, defined by holding the same potential,

$$W(x, y, z) = constant.$$

The Geoid is an equipotential surface which coincides with the mean sea level, and this surface can be used as a reference surface for height system in any part of the world. If the height is referred to an equipotential surface, the height in a position is related to the potential in that spot, and thus the gravity.

A spirit level will always coincide with the equipotential surfaces, or level surfaces, and the direction of the gravity vector will be orthogonal to these surfaces at any point along the surface. In the vertical direction these lines need not be straight, as the potential differ with the equipotential surfaces which are not parallel. The lines of force are called *plumb lines*. The gravity vector will in any point follow the tangent of the plumb line. The distance between the equipotential surfaces corresponds to change in gravity.

A method to study heights is to implement the gravity potential W. With respect to a reference potential W_0, the height of a point P is given by the potential difference to the reference surface. This difference is denoted the geopotential number C (Torge, 2001), and this makes height a physical, rather than a geometric measurement.

$$C = W_0 - W_P. \tag{3.11}$$

3.3 Geophysical effects

Equation (3.1) displays the connections between two masses and the distance between them. Even though the Sun is several times larger than the Moon, the Moon still

Table 3.1: Principal gravimetric partial tides for $\overline{\phi} = 45\,\text{deg}, h = 0$ (Torge, 2001).

Symbol	Name	Period
M2	Main moon tide	12.42 h
S2	Main sun tide	12.00 h
K1	Main diurnals decl. tide	23.93 h
O1	Main diurnal moon tide	25.82 h
N2	Ellipt. tide to M2	12.66 h
P1	Main diurnal sun tide	24.07 h
K2	Declin. tide to M2, S2	11.97 h
Q1	Ellipt. tide to O1	25.82 h
Mf	Declin. tide to M0	13.66 d
Mma	Ellipt. tide to M0	27.55 d
Ssa	Declin. tide to S0	182.62 d

affects the gravity field of the Earth much more than the Sun because of its vicinity. The lunisolar gravitation affects the masses and gravity of the Earth (Fig. 3.1), and the tides occur in both the oceans and the atmosphere, as well as in the solid Earth itself. A number of factors are affecting og deforming the Earth at all times. Earth reacts as an elastic body, with different elasticity in the different matters (air, fluids, solid Earth). The influencing parameters (Tab. 3.1) affect the geodetic measurements and result in gravity changes that must be reduced for in time-independent modelling.

Earth Tide

The ephemerides of the Sun, the Moon and the planets in the solar system can be used for calculations of the tidal effect. The reaction and deformation of the solid Earth's surface to these parameters is called Earth tide (Fig. 3.1). Tidal variations will also be found in the oceans and in the atmosphere.

The gravitational potential on the surface of Earth is affected by the tidal-induced change of masses in vertical direction. These deformations can be represented mathematically and estimated in the magnitude of a few decimeter in height and 1 to 2 $\mu m/s^2$ in gravity (Torge, 2001).

Models of solid Earth exist and are being validated and improved continuously, and these models contribute to satisfactorily reducing geodetic measurements.

Ocean Tidal Loading

Caused by the ocean tides, the direct attraction of the water masses induces a loading effect on the surface of the Earth called the ocean tidal loading. Close to the coast this loading effect comprise up to 10 % of the gravitational signal. Ocean loading can be modelled based on the ocean tide models and the equations of hydrodynamics

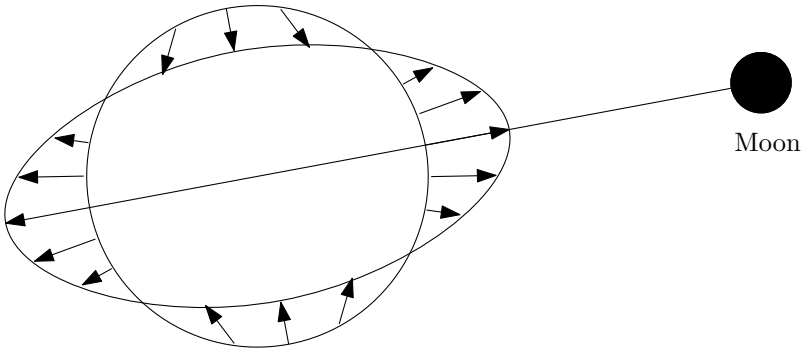

Figure 3.1: Tidal accelerations affected by the Moon (Torge, 2001)

together with tide observations, and it is calculated as a response of an elastic body to a point load (Torge, 2001)

Polar Motion

The deviation of the rotational pole relative to the reference pole of the International Earth Rotation and Reference System Service (IERS) is called polar motion (Fig. 3.2). The motion mainly consists of two periodic components and one long-term irregular drift. The Chandler period (the wobble) has a period of 435 days with an amplitude of about 3 - 6 m. The period is induced by dynamic flattening of the Earth, and mass displacements in both atmosphere and oceans affect the wobble continuously. Seasonal variations in the atmosphere and the oceans cause an annual period with amplitudes of magnitude of 1.5 - 3 m. The secular motion of the pole, the drift, is assumed to be caused by post glacial uplifts in northern Canada and Europe. The polar wander has a magnitude of 0.1 m per year (Timmen, 2010).

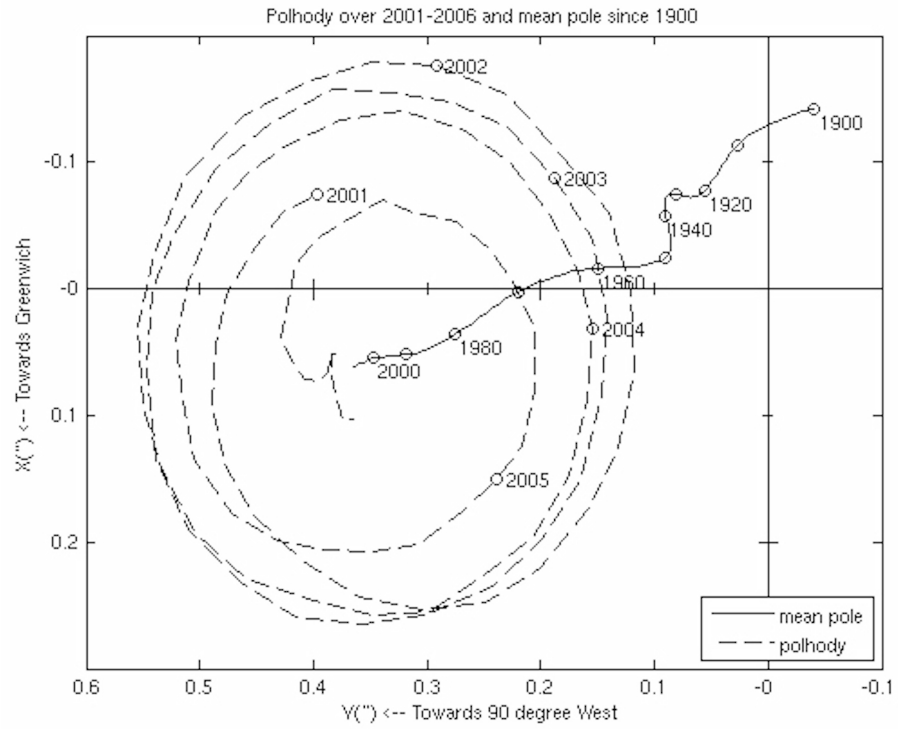

Figure 3.2: Polar motion (NASA, 2014)

3.4 Gravimetry

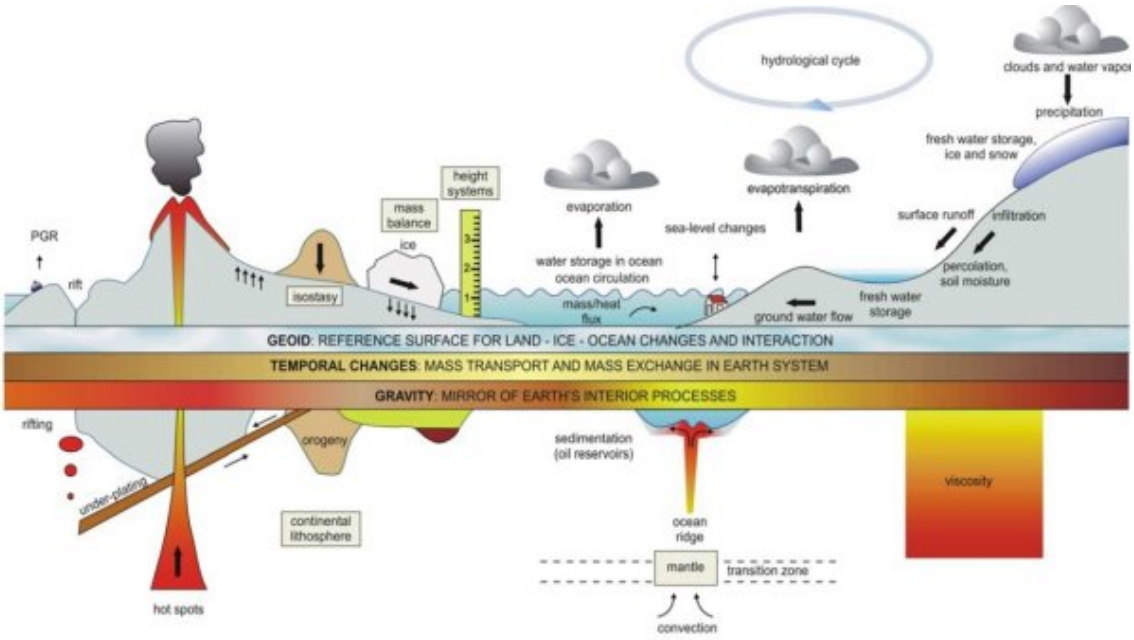

Figure 3.3: Mass transport of the Earth systems (IAG, 2014)

The applications of gravimetry span different disciplines and fields of study (Fig. 3.3), and a few of the applications are mentioned below:

- Geoid computation
- Definition and modelling of vertical reference frames
- Observation and modelling of earth tides
- Observation of vertical crustal motion and related mass redistribution
- Observation of mass distribution in the earth system

Historically, a pendulum (Fig. 3.4) was used for gravimetric measurements, and this is one of the basic physical principles of measuring gravity. The pendulum is a massive bob attached to a massless rod hanging in a frictionless pivot. From its equilibrium position, the bob is shifted to an amplitude and the gravity accelerates the bob towards the equilibrium position where it will oscillate. Without air friction, this oscillation will continue indefinitely with constant amplitude (Fig. 3.4).

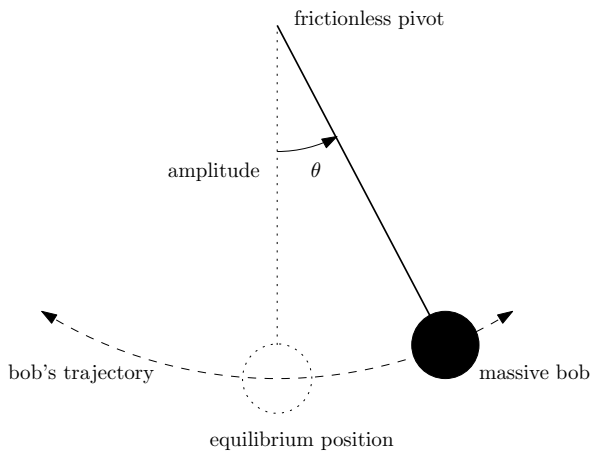

Figure 3.4: Pendulum principle

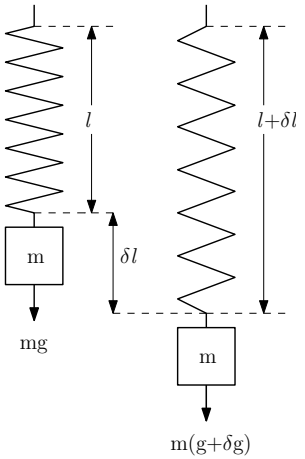

Figure 3.5: Spring principle

For small amplitudes, the period T of a pendulum, as described in Figure 3.4, can be expressed by the length L of the rod and the acceleration of gravity g in a position can be derived from

$$T = 2\pi\sqrt{\frac{L}{g}}. \tag{3.12}$$

The spring based relative gravimeter was introduced around 1930. The principle is based on Hooke's law,

$$F = k\,l, \tag{3.13}$$

where F denotes the force needed to influence the extension l of the spring (Fig. 3.5). The two quantities are proportional to each other and only scaled by the spring characteristic k.

As the spring is affected by the local gravity, the mass shifts its position. The force needed to put the mass back in its original position or to the equilibrium state, line reflects the gravity in the position (Fig. 3.5).

Free-fall and rise-and-fall instruments were introduced around 1960 and made it possible to measure absolute gravity values. The principle is based on time and positioning from a free falling mass, like Newton's apple.

Terrestrial measurements as well as satellite observations and observations from aeroplanes are now available and offer several opportunities to observe the Earth's gravity field.

As the gravimeters are very sensitive to the surrounding mass, variations and shifts in the mass balance near by will have an effect on the measurements. This will include the atmosphere and the hydrosphere as well as mass shifts within the Earth's crust. With the necessary high precision positioning of the measuring point, changes in height due to crustal deformations or change in distance to the Earth's rotation pole can be derived from long-time measuring series (Timmen, 2010). Magnitudes of some gravitational signals is listed in Table 3.2.

In geodesy the SI units for acceleration m/s^2 is substituted by Gal (1 Gal = 1 cm/s^2), named after the Italian physicist and astronomer Galileo Galilei.

$$1mGal = 10^{-5} m/s^2 = 10^{-6} g$$
$$1\mu Gal = 10^{-8} m/s^2 = 10^{-9} g$$

Table 3.2: Magnitude of some gravitational signals (Wenzel, 1997) (Breili, 2009)

Acceleration m/s^2	
10	Gravitation of the Earth
10^{-2}	The Earth flattening and rotation
10^{-3}	Mountains and ocean trenches
10^{-4}	Internal mass distribution
10^{-5}	Large reservoirs
10^{-6}	Tidal acceleration from the Sun and the Moon
	Distant Earthquakes
10^{-7}	Changes in the Earth cryosphere
	Hydrological change
	Ocean tide loading and costal stations
10^{-8}	Ocean tide loading far from the coast
	Nearby large buildings
	Annual post glacial rebound
	Polar tides
	Atmospheric loading
$10^{-11} - 10^{-20}$	Tidal acceleration from the planets

3.4.1 Relative gravimetry

With relative gravimetry variations in gravity in space and/or time can be observed. With an absolute gravity value measured on a position, relative gravimetry can connect gravity values to other stations. Additionally, it can be used to locate differences in the same position in long time-series and to define the gravity gradient.

Spring gravimetry

Due to the elastic spring and its properties, the instrument with its interior must be kept under steady conditions. Temperature changes, small shocks or vibrations will however, influence the mechanical parts in the instrument and cause a drift. For stationary measurements, the drift is close to linear, but field work will affect the instrument and the drift need to be modelled. Drift is also caused by ageing of the spring. Determination of the drift can be modelled by repeatedly measuring in the same position during a set, and methods for this exist (Fig. 3.6). The profile method can be described as measuring along a profile and repeat some of the positions after finishing, going in the backward direction. The step method is more robust for drift control as the time differences between reoccupations are shorter. The main difference is however, that when using the profile method the operator ends up at the starting point (Timmen, 2010).

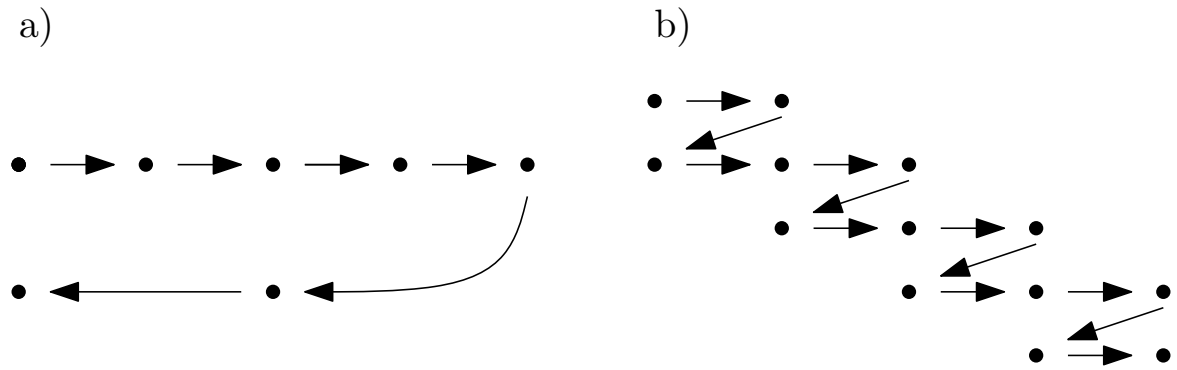

Figure 3.6: Methods for drift control a) the profile method, b) the step method

LaCoste & Romberg Gravity Meter

The LaCoste and Romberg-instrument is a spring-based relative gravimeter. In this instrument, a test mass is supported by an elastic spring connected to an advanced gear system with numbering called the counter unit. When the gravity acceleration changes or the instrument is placed in a new position, the operator shifts a numbered wheel on top of the instrument to fit the local gravity conditions. Through a gear system, the suspension point of the spring is shifted such that the test mass is placed at the reference point. When the test mass is in the reference position and the force in the spring equals the gravity affecting the test mass, the operator reads the value from the counter unit. The instrument at NMBU has an electronic feedback system inserted, and the operator can read the values directly from a display or connect the instrument to a logging device.

The observation equation (eq. 3.14) connects the raw readings to the resulting gravity value for a LaCoste & Romberg relative gravimeter. The counter units need to be calibrated to a gravity value, with some already known parameters. The calibration between the counter units and the gravity value has to be known, as well as the drift.

$$g = N_0 + \sum_{j=1}^{p} d_j (t - t_0)^j + \sum_{k=1}^{m} Y_k z^k + \sum_{l=1}^{n} A_l \cos(\omega_l z - \phi_l) \tag{3.14}$$

where N_0 refers to the instrument level, d_j = drift parameter of degree j, t_0 = starting time of the first measurement, Y_k = calibration coefficient of degree k, z = reading in counter units, A_l = amplitude, ω_l = frequency, ϕ_l = phase of the periodic term of degree l (Timmen, 2010).

ZLS Burris Gravity Meter

The Burris Gravity Meter is based on the LaCoste & Romberg system, with a digital feedback range of 500 μms^{-2} (Torge, 2001). The instrument has no display. The operator reads from an electronic notebook, and the instrument gives statistical measurements directly to the field log. Similarly to the LaCoste & Romberg Gravity Meter the operator calibrates the counter unit to fit the local gravity conditions. The instrument stores the data and displays the results on the remote palmtop.

3.4.2 Absolute gravimetry

For this thesis, the FG5-226 constructed by Micro-g Lacoste (USA) was used. The instrument will be described in this section and will from here be denoted FG5. The FG5 is one of the instruments produced with the highest precision available to measure the absolute gravity acceleration. The instrument is a free-fall instrument, and the principle (Fig. 3.7) is based on time and distance measurements along the vertical direction.

The lower part of the instrument consists of a super-spring holding a reflector still, eliminating vibrations in the ground below the instrument and the interferometer. The upper part of the instrument has no contact with the lower part and holds a vacuum chamber with a reflecting test mass able to fall freely. A iodine stabilized laser is an exterior part of the instrument.

The interferometer is an optical chamber where the incoming laser beam is split into a reference beam and a test beam. The test beam is reflected up into the upper part of the instrument, reflecting off the falling test mass, and it then reflects off the reflector in the lower chamber, and is measured against the reference beam in the photo detector. The reference beam's path is directly through the interferometer to the photo detector. Together with a rubidium oscillator the two signals are then measured against each other.

Equation 3.15 of motion is used for deriving the gravity acceleration

$$m\frac{d^2z}{dt^2} = m\ddot{z} = mg \tag{3.15}$$

where z is the vertical axis, m is the mass of the reflecting test mass and t is the time.

There must be at least three measurements to solve the gravity component. In the vacuum chamber however, the trajectory of the falling mass is measured at 700 fringes. The time-distance-data is set to a fitting curve (see Fig. 3.8) and gives the gravity acceleration in the reference height, $g_0 = g$.

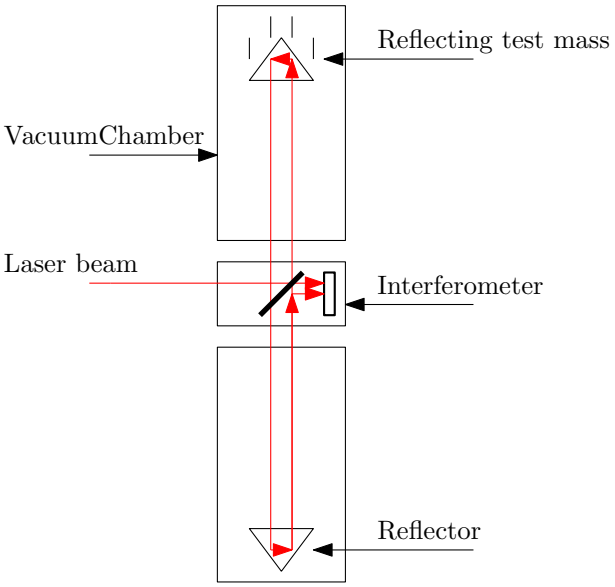

Figure 3.7: Measuring principle of FG5 (Microg-Lacoste, 2014)

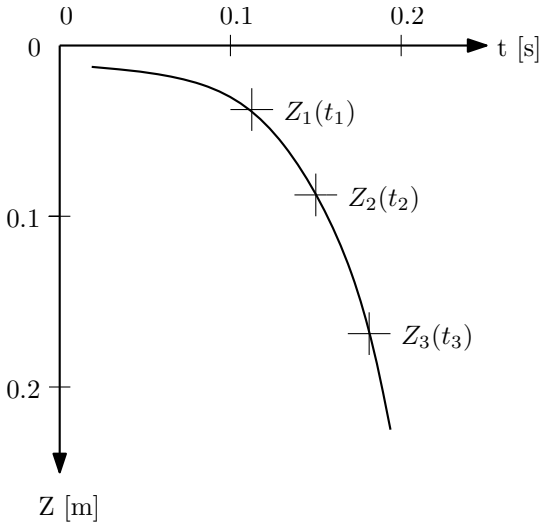

Figure 3.8: Time-distance diagram of a free-fall (Microg-Lacoste, 2014)

Considering that the gravity field is not homogeneous in vertical direction, a more precise accuracy can be given with implementing the gravity gradient. Equation (3.15) must be read as

$$m\frac{d^2z}{dt^2} = m\ddot{z} = m(g_0 + g_z z), \tag{3.16}$$

where $g_0 = g$ in the zero position $z = 0$.

$$z = \frac{g_0}{g_z}(cosh\sqrt{g_z}t - 1) \tag{3.17}$$

The observation equation is then derived as a series development of z (Torge, 2001)

$$z = z_0\left(1 + \frac{1}{2}g_z t^2\right) + z_0\left(t + \frac{1}{6}g_z t^3\right) + \frac{1}{2}\dot{g_0}\left(t^2 + \frac{1}{12}g_z t^4\right) + ... \tag{3.18}$$

The gravity gradient in the point is measured and used to calculate changes in the gravity value in vertical direction. This is done by measuring several sets of gravity values in different elevations along the same vertical direction with a relative gravimeter. The average of these measurements defines the gradient

$$Gradient = \frac{\Delta g}{\Delta H} \tag{3.19}$$

The FG5 instrument is capable of measuring the gravity acceleration with the precision of the 8^{th} digit, μGal.

3.4.3 Satellite gravimetry

Dedicated gravity satellite missions have given the opportunity to make global measurements of the Earth's gravity field. With precise theoretically satellite orbits, perturbations (deviations from the theoretically and the observed orbit) are used to derive the Earth's gravity field. Three main measurement principles are developed; high-low satellite-to-satellite tracking, low-low satellite-to-satellite tracking and gradiometry. The high-low satellite-to-satellite tracking method is based on GNSS (Global Navigation Satellite System) observations from a satellite in a low orbit. With the availability to track the position of the satellite in three dimensions from measurements of GNSS satellites flying in a higher orbit, and measurements from an accelerometer placed in the centre of mass of the satellite, forces affecting the satellite can be compensated for. The low-low satellite-to-satellite tracking method is based on differentiation, where the distance between the satellite pair is measured with high precision. Mass anomalis on the surface (e.g. mountainous areas) will affect the gravity acceleration of one satellite

and thereby affect the distance between the satellite pair. From the distance measurements the gravity field can be derived. Gradiometry is the most advanced method, based on GNSS positioning and six accelerometers placed around the centre of mass of the satellite, along each of the three orthogonal axis. The affecting forces can be corrected for and changes in the gravity field can be detected in three dimensions (Fig. 3.9).

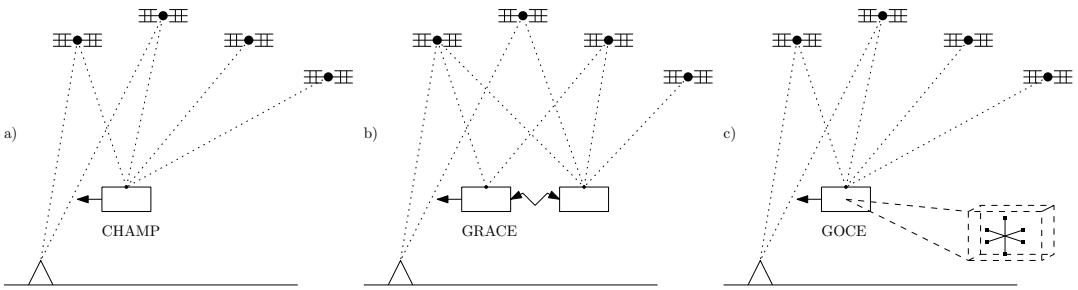

Figure 3.9: Measuring methods for observing the Earth's gravity field from space. a) High-low satellite-to-satellite tracking. b) Low-low satellite-to-satellite tracking. c) Gradiometry

Three satellite missions implemented with the three different measuring principles have been launched. *CHAMP - CHAllenging Mini-satellite Payload* launched in 2000, was the first satellite constructed to measure the Earth's gravity field. The mission was based on the high-low satellite-to-satellite method. *GRACE - Gravity Recovery and Climate Experiment* launched in 2002, used the low-low satellite-to-satellite method for observations of the Earth's gravity field. The distance between the two satellites following each other in the same orbit were about 220 km. *GOCE - Gravity and Ocean Circulation Explorer* launched in 2009 used the gradiometric method for observing the Earth's gravity field (Lysaker, 2011).

3.5 Gravity anomalies and terrain effects

Terrain modelling

The gravitational potential from a rectangular prism (eq. 3.20) can be calculated, based on the law of gravitation (eq. 3.1). Input parameters are the gravitational constant G, the , dx dy dz, of the prism, the density ρ of the mass, and the vector from each mass element of the prism to the calculation point, $\sqrt{x^2 + y^2 + z^2}$ (Fig. 3.10). Such prisms can model the irregular geometry (heights) of the topography, and fit the purpose of modelling digital elevation models which are given in gridded forms.

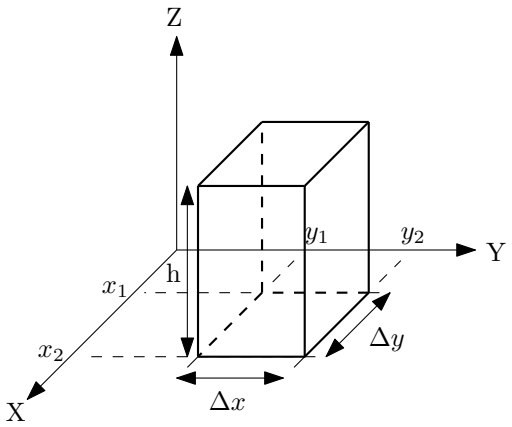

Figure 3.10: Rectangular prism method for calculation of gravitation of topography

$$V_{top} = G\rho \int_{x1}^{x2} \int_{y1}^{y2} \int_{z1}^{z2} \frac{dxdydz}{\sqrt{x^2 + y^2 + z^2}} \tag{3.20}$$

The vertical component of the gravitation is given by

$$b_z^{prism} = G\rho \left| \left| \left| xln(y + r) + yln(x + r) - z \cdot arctan\frac{xy}{zl} \right|_{x1}^{x1} \right|_{y1}^{y2} \right|_{z1}^{z2} \tag{3.21}$$

where the r is the length of the vector from centre of the prism to the calculation point ($r = \sqrt{x^2 + y^2 + z^2}$) (Nagy, 1966).

The total effect of the gravitation on the calculation point is given by the sum of the gravitation of all the individual prisms,

$$\delta g_{top} = \sum b_z \tag{3.22}$$

Terrain correction

Terrain correction is removing irregularities of the topography. With creating plates of constant thickness and density, where mass deficits below a point are filled in, and where mass excess above the point are removed, a curved surface can be modelled by an easier formation (Fig. 3.11).

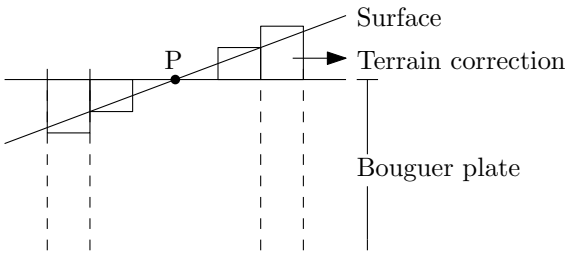

Figure 3.11: Bouguer plate and terrain correction

Removing the effect of the topography with a topographic reduction δg_{top}, the Bouguer gravity anomaly Δg_B is obtained. The topographic reduction is the total effect of topography (Torge, 2001).

$$\Delta g_B = g - \delta g_{top} \tag{3.23}$$

4 — Establishing gravity values

Preparations at Svartisen Subglacial Laboratory

In preparation for the field work planned for this thesis, a pillar for placing the FG5 instrument on in the subglacial laboratory was built in September 2013. This work was done by Christian Gerlach, Torsten Spohnholtz and Siri Eikerol, together with Miriam Jackson from NVE as responsible for the Subglacial laboratory.

The pillar was made of rock and cement in a construction form work (Fig. 4.1). The placement of the pillar was decided by the height from the flooring to the ground rock and the ability to control the indoor conditions. A marker was placed in the middle of the pillar to define the gravity station (Fig. 4.2). The form work was built separately from the surrounding housing to eliminate vibrations, and the pillar was built in contact with the ground rock. To control the air flow, insulation was placed between the housing and the form work, however, the pillar should not be affected by vibrations in the surrounding house. The insulation layer could be shifted at any time if necessary. The flooring panel was placed on top after measurements and the floor can be used as normal.

Figure 4.1: The form work of the FG5-pillar

Figure 4.2: Marker for the FG5-pillar

Coordinates from the construction of the tunnel existed as analogue coordinates. These were digitalized from pictures of coordinate list (Fig. 4.3), and used as a help for planning the surveying of the tunnel.

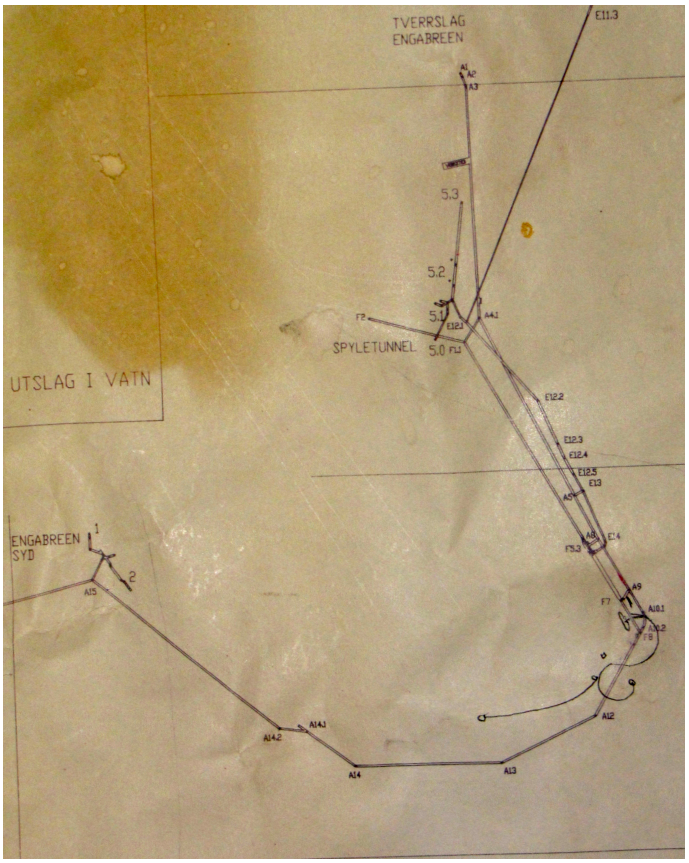

Figure 4.3: Old map of the tunnel system (Photo: Christian Gerlach)

Preparations at NMBU

The FG5 is a very sensitive instrument and is dependent upon the operator to be consistent through measuring sessions to achieve comparable results. In January and February 2014, many hours were spent on practising operating the instrument in the measuring laboratory at NMBU. To be able to bring the instrument into the subglacial laboratory a lot af training was needed to diagnose and troubleshoot, as well as for assembling the instrument. Together with master student, Alexander Helland, and PhD student, Vegard Ophaug, a step-by-step booklet was written for everyone's use when setting up the instrument.

To calibrate the rubidium oscillator, the instrument was brought to the Norwegian Metrology Service in February 2014. The absolute gravity acceleration was measured in one of their laboratories, as well as three gradients in three different laboratories.

4.1 Field methods

The work in the tunnel was conducted during March 18th - 23rd, 2014. Participants were Siri Eikerol, Christian Gerlach, Alexander Helland, Miriam Jackson and Vegard

Ophaug.

To get as long measuring period as possible, it was crucial to assemble the absolute gravimeter as one of the first actions. The gradient on the absolute gravity station was measured before mounting the instrument. Two measuring sessions were conducted during the mission, first a session of 48 hours and next a session of 24 hours, giving a total of 72 hours of measurements.

A survey of the tunnel was performed to establish coordinates for gravity measurement stations (Fig. 4.4, Fig. 4.5). A net of four GNSS stations were set outside the main entrance. From this net, surveying was done in towards the tunnel, to the pillar and further through the water tunnel to the exit on the other side of Engabreen glacial outlet. During two days, a survey of the whole tunnel section was performed, altogether about three kilometres from the entrance to the exit on the other side of the glacier. A GNSS station was also placed in the tunnel exit to ensure better geometry of the survey. Gravimeter stations were marked by inserting a bolt in the tunnel wall, as well as marked with paint for easy access at later missions. Around the laboratory, three gravity measuring stations were placed as control to the absolute value from the FG5 observations. The control stations are not necessary for the mass balance studies; therefore only two of these stations (G14 and G15-1) have horizontal coordinates. When adjusting the survey, the datum was set to EUREF89 and the heights were referred to ortometric heights calculated for the given coordinates on an internet based service (Geographiclib, 2014).

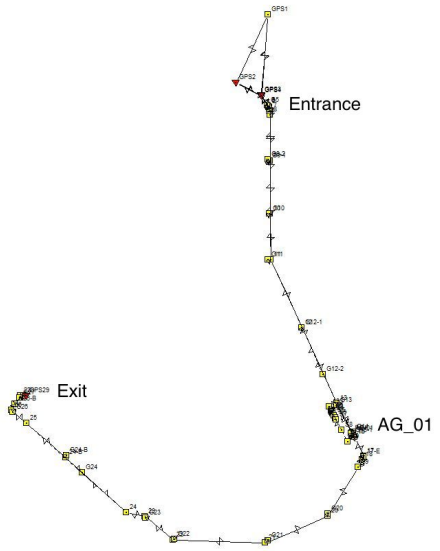

Figure 4.4: Survey plot of the whole tunnel section, GisLine

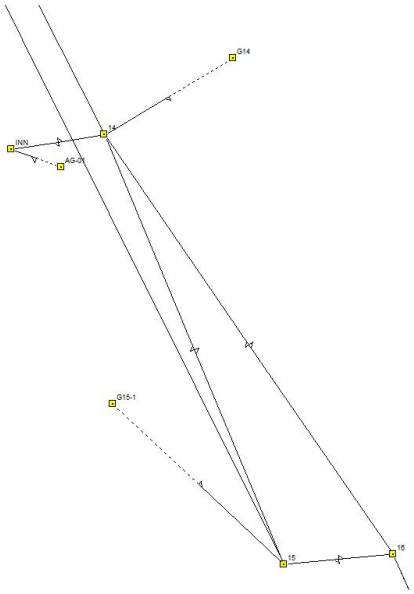

Figure 4.5: Plot of the positions around the FG5 pillar, GisLine

Levelling was done from the tunnel entrance to the laboratory, but due to poor light conditions, the results were omitted.

The relative gravity values were measured on the last day of the mission. The measuring started at gravity station G15-1, one of the surrounding points of AG_01, and

then through the water tunnel to the exit and gravity station G27. Measurements were taken at every gravity station. To control for drift, two stations were measured also when returning to the pillar. Measurements were likewise done from gravity station AG_01 to G5 at the tunnel entrance and back to AG_01. Several stations were measured twice for drift control between stations AG_01 and G5.

Measurements were done with a LaCoste & Romberg (LCR G-761) relative gravimeter and a Burris Gravity meter (ZLS B-78). The instruments were transported in customized backpacks to ease the walk in the tunnel. Because of poor connection between the LCR relative gravimeter and its changable battery, the temperature gradually decreased during the measurements. When unpacking the instrument at some stations, it was observed that the power had been cut during transportation from the previous station. This instrument was set to power in the laboratory and was not used for the measurements between the entrance and laboratory.

The personnel and all the equipment were flown by helicopter to the tunnel entrance both when arriving and departing the mission.

4.2 Data analysis

Analysis of the collected data from March 2014 was processed at NMBU.

4.2.1 Gravity gradient

The gravity gradient on the pillar in the laboratory was measured using the LCR G-761. This was done by successively measuring on top of a tripod and on the pillar surface 11 times during a time period of approximately one hour. The height of the tripod was 1.4 m. One of the measurements was discarded because of external noise.

The average μ and the standard deviation S_0 of the observations were calculated on site:

$$\mu = \frac{1}{n}\sum_{i=1}^{n} x_i \tag{4.1}$$

$$S_0 = \sqrt{\frac{1}{n-1}\sum_{i=1}^{n}(x_1 - \mu)^2} \tag{4.2}$$

The standard deviation of the mean is calculated with the following equation

$$\overline{S_0} = \frac{S_0}{\sqrt{n}} \tag{4.3}$$

Table 4.1 presents the gravity gradient for gravity station AG_01.

Table 4.1: Gravity gradient for AG_01, March 18, 2014

	mGal/m	μGal/cm
Gravity gradient	0.2429	-2.4
Standard deviation	0.0047	0.047

4.2.2 Absolute values

The gravity measurements at gravity station AG_01 (Table 4.2) have been reprocessed with final parameters in the processing software following the instrument package, g9. Final polar coordinates were given as input as well as the gravity gradient. The software calculates Earth tide parameters and the nominal air pressure from coordinates and height of the examination point. The nominal pressure is the long term mean pressure at the given coordinates, however, the instrument also provides a barometric pressure correction. By comparing the two values the gravity value is corrected in the software to estimate the value on a "normal" day (Microg-LaCoste, 2012).

Table 4.2: Coordinates of the absolute gravity station

Station	Latitude	Longitude	Orthometric height
AG_01	66° 40' 25.8420" N	13° 47' 44.7503" E	609 m

Final polar coordinates (Table 4.3) were downloaded from Micro-g LaCoste' internet pages (www.microglacoste.com). Two measuring sessions were conducted at two different dates and with different number of sets (Table 4.4).

Table 4.3: Final polar coordinates

Date	X	Y
March 19th	0.0254	0.4060
March 20th	0.0262	0.4065
March 21st	0.0274	0.4071
March 22nd	0.0283	0.4084

Table 4.4: Number of observed sets, number of drops in each set and the sampling interval

Sampling session	Set interval	Drop interval	# sets	# drop
March 19th	60 min	10 sec	48	50
March 22nd	60 min	10 sec	24	50

The reference height of the absolute values in FG5 is 1.2 m above ground level. To lower this value to the ground level the gravity gradient is multiplied with the reference height. The uncertainties of the measurements at ground level are calculated with the standard deviation of the gravity gradient together with the uncertainties of the absolute measurements

$$\sigma = \sqrt{(h\sigma_{gradient})^2 + \sigma_{FG5}^2} \tag{4.4}$$

Processing with g9 software

Initial processing of the absolute value was done with the default settings in the software. Plotting the residual signal (the difference between the actual fringe time and the least squares fit estimate of the positon at that time) (Microg-LaCoste, 2012) from a single drop shows at which fringe the test mass hits the elevating carriage. The drop fit (Table 4.5) was set to be values which excludes collisions between the test mass and the carriage

Table 4.5: Drop fit interval of the FG5 sessions

Start time (ms):	35.03	Stop time (ms):	150.06
Start fringe:	19	Total fringes:	331

The default tidal corrections is the ETGTAB model for Earth tide and the model of Schwiderski for ocean loading (Microg-LaCoste, 2012). Comparisons of the gravity sets and the set corrections showed a correlation between the ocean loading and the set measurements along the time axis. In order to preclude this correlation, reprocessing with the three different ocean loading models available in the software as well as no active ocean loading model was conducted.

The differences in the ocean loading models implemented in the g9 software are the long-periodic parameters. The Schwiderski model includes all parameters in the model, whereas the FES2004 and the CRS3.0 exclude the long-periodic parameters, Mf, Mma and Ssa (Table 3.1).

Table 4.6: Gravity and uncertainties using different Ocean loading models (all sets included)

Sampling session	Ocean loading model	Gravity	Set scatter
March 19th	Schwiderski	982202710.92	4.24
	FES2004	982202710.34	3.09
	CRS3.0	982202710.52	4.02
	No model	982202710.04	4.11
March 22nd	Schwiderski	982202708.46	3.65
	FES2004	982202708.54	4.17
	CRS3.0	982202708.40	3.60
	No model	982202708.80	5.70

Given the number of sets in each sampling session the absolute value with the ocean loading model from FES2004 was chosen to give the best results due to the low set scatter in the session from March 19th (Table 4.6). A weighed mean value (eq. 4.5, eq. 4.6) for the two gravity values (Table 4.7) corrected by the FES2004 model and a weighed standard deviation are presented as a final gravity value in station AG_01 in Table 4.8. The two sessions were processed with final polar coordinates to the correct dates.

$$w_i = \frac{1}{s_0^2} \qquad \overline{g} = \frac{\sum_{i=1}^{n} w_i g_i}{\sum_{i=1}^{n} w_i} \qquad (4.5) \qquad \overline{s_0} = \sqrt{\frac{1}{\sum_{i=1}^{n} w_i}} \qquad (4.6)$$

Table 4.7: Absolute gravity values from measuring sessions

Session		μGal
March 19th	Gravity	982202710.18
	Set scatter	3.08
March 22nd	Gravity	982202708.54
	Set scatter	4.17

The two sampling sessions were merged with the additional utility "gProjectMerge" following the g9 software to calculate a resultant gravity value based on all sets. The Ocean loading model for the merging option was set to FES2004, and the rest of the parameters were equal to the previous processing. Polar coordinates were set to values for March 21st, the mid day of the two sessions and a separate pocessing were also done without a group of sets which in the plotted gravity sets distinguished from the other (Fig. 4.6), these were sets 33-37 and set 59. Efforts were taken to find possible reasons for the distinguished sets, such as controlling for earthquakes on the internet pages of the United States Geological Survey(USGS, 2014)) and relating to persons using the laboratory housings at the given time. No match for either earthquake or human interference were found. The final gravity values are presented in Table 4.8.

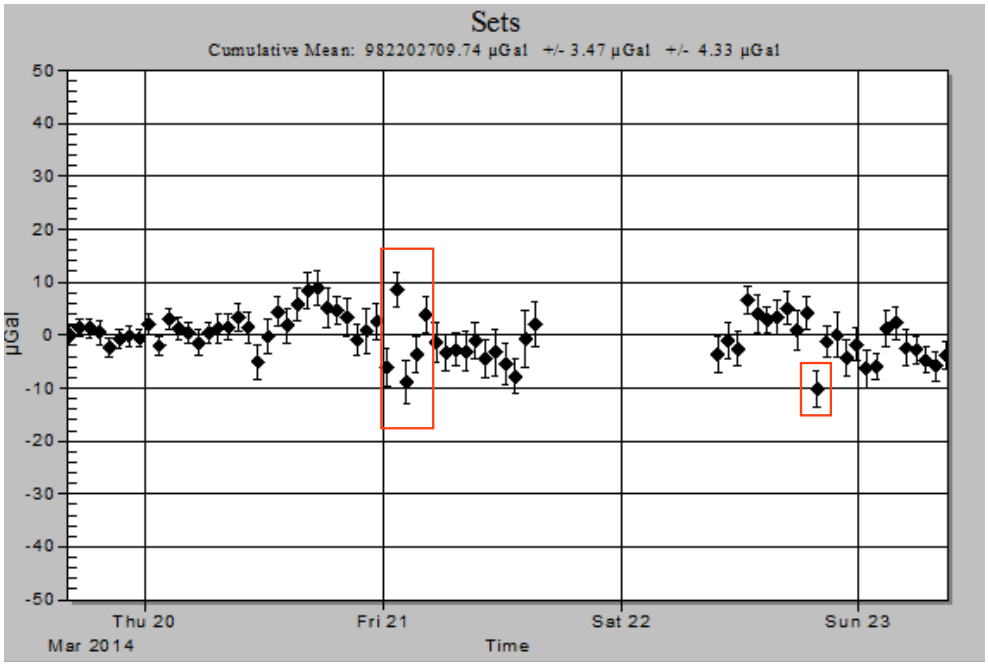

Figure 4.6: Gravity set from both sampling session. The drops marked in squares were excluded from processing

Table 4.8: Absolute gravity values in station AG_01, results from different processings.

Gravity	Set scatter		Comments:
982202709.50	2.47	μ Gal	Mean value (extracted from Table. 4.7)
982202709.74	3.47	μ Gal	Merged: all drops included
982202709.86	3.15	μ Gal	Merged:excluded drops: 33, 34, 35, 36, 37, 59

The resulting uncertainty of the mean value is smaller than the uncertainties given directly from the processing software for the merged sessions. With equation 4.6 random error is assumed, however this value might be unrealistically small as the processing software g9 adds constants to the error budget (Microg-LaCoste, 2012). This result is omitted and the result from the merged session with all drops included is identified as the final gravity value for gravity station AG_01:

$$982202709.74 \pm 3.47 \mu Gal$$

4.2.3 Relative values

The raw gravity observations obtained from the relative gravimeters needed to be reduced for Earth tides. The reductions can be downloaded from http://www.bfo.geophys.uni-stuttgart.de/etgtab.html. Specifications for position and the wanted period must be set and the program computes astronomical and geodetic elements and the tidal amplitudes, the latter from the potential development. The program was written by Dr.-Ing.habil Hans Georg Wenzel at the University in Karlsruhe.(REF:ETGTAB.TXT)

Drift control

In both directions, to the exit of the tunnel and to the entrance from the pillar, stations were measured twice to control for instrumental drift as described in section 3.4.1. The mean value for each station was calculated and each value was reduced with the mean corresponding to the station. This leaves only the drift in the units of mGal and the values could be plotted along a time axis for control.

Figure 4.7 shows the reduced readings and residuals for LCR G-761 measurements plotted along a time axis and Figure 4.8 show the reduced readings and residuals for ZLS B-78. The values presented in Fig. 4.8 do not correlate to a linear drift trend and separate plots were made for the time period between 10:00 and 17:30 (Fig. 4.9) and 18:00 and 23:40 (Fig. 4.10) due to measuring break at that time. However, the drift plot shows two separate trends in the time periods 18:00 to 20:00 and 20:00 to 23:40. Figure 4.11 and Figure 4.12 shows linear drift trends and these time periods were used in the adjustment computations. The separated time periods correlated with three different transportation methods for the ZLS instrument. While the instrument was carried in a backpack between 11:30 and 18:00, for the time period 1800 to 20:00 it was only transported for repetitions of close laying gravity stations and no repacking was needed. For the last time period the instrument was carried to the tunnel entrance with no repacking, but here the distances between the gravity stations are longer. For the three linear drift trends, the residuals did not exceeds 15 μGal for any of the two instruments.

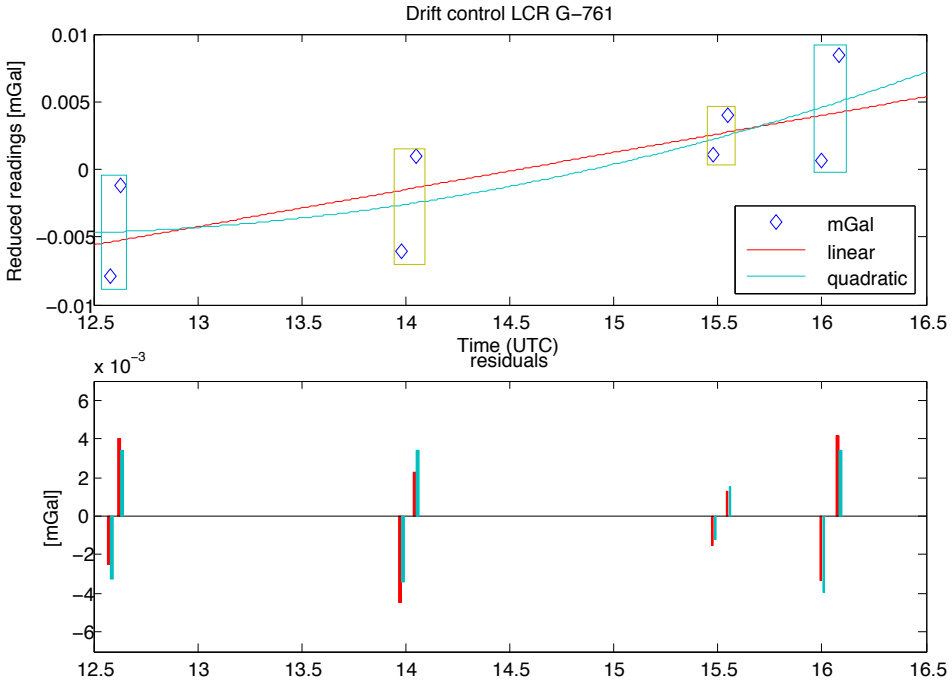

Figure 4.7: Reduced gravity readings by LCR G-761 for the time period 10:00 to 17:30 for gravity stations G22 and G24-B

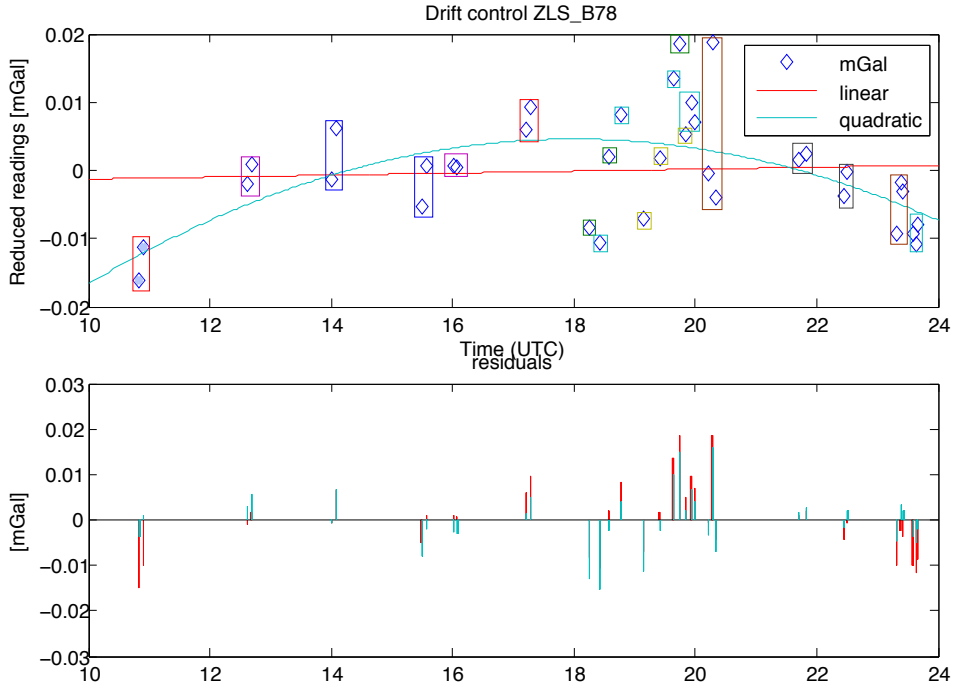

Figure 4.8: Reduced gravity readings by ZLS B-78 for the time period 10:00 to 23:40. Gravity stations: G09-2, G13, G15-1, G15-2, G22, G24-B and AG_01

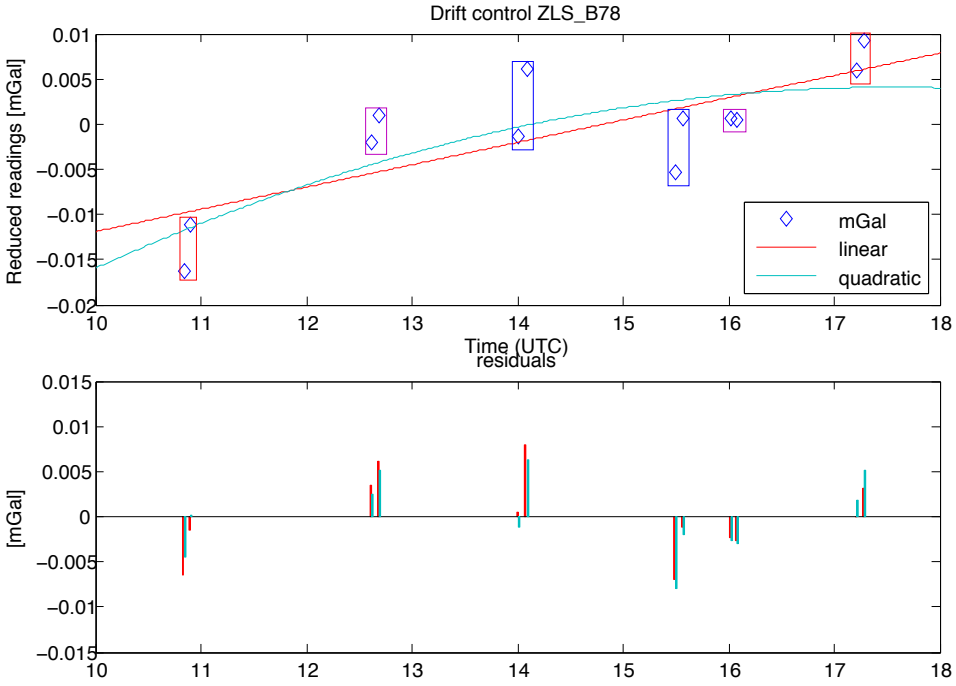

Figure 4.9: Reduced gravity readings by ZLS B-78 for the time period 10:00 to 17:30. Gravity stations: G15-1, G22, and G24-B

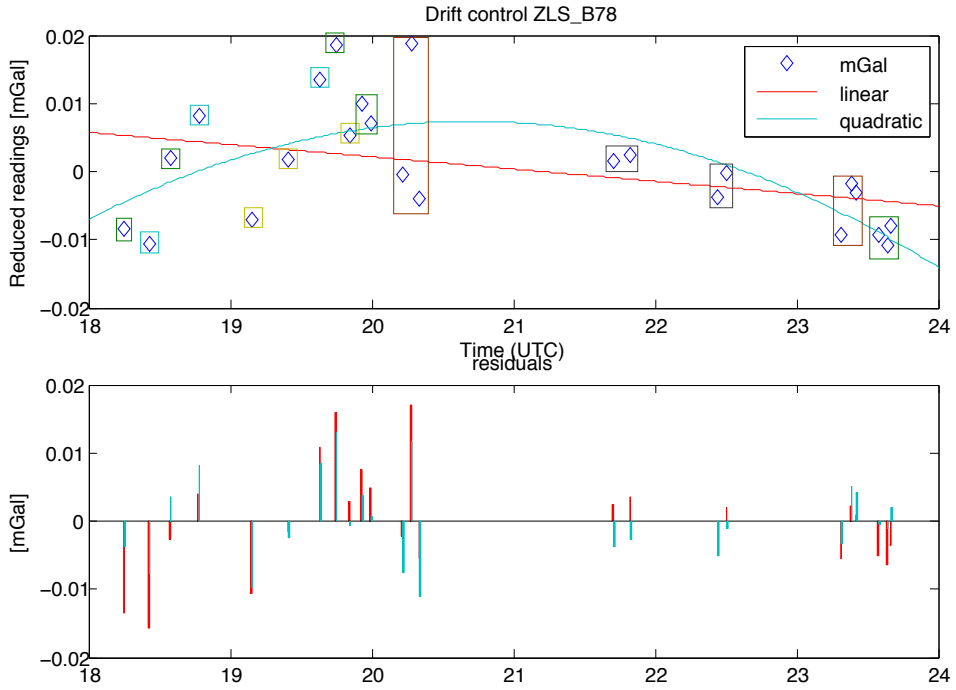

Figure 4.10: Reduced gravity readings by ZLS B-78 for the time period 18:00 to 23:40. Gravity stations: G09-2, G13, G15-1, G15-2 and AG_01

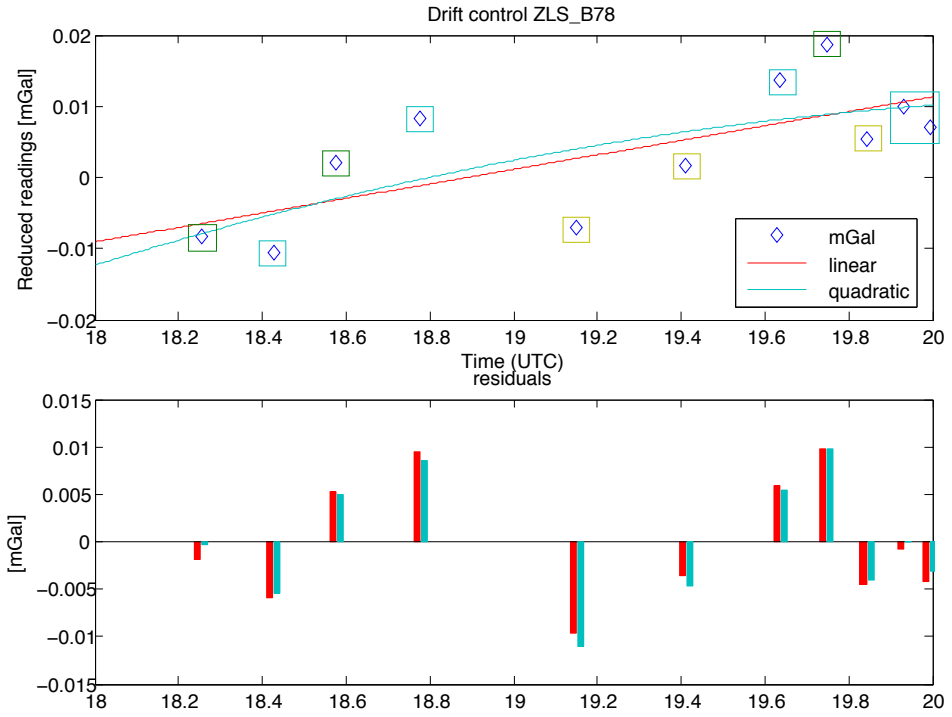

Figure 4.11: Reduced gravity readings by ZLS B-78 for the time period 18:00 to 20:00. Gravity stations: G15-1, G15-2 and AG_01

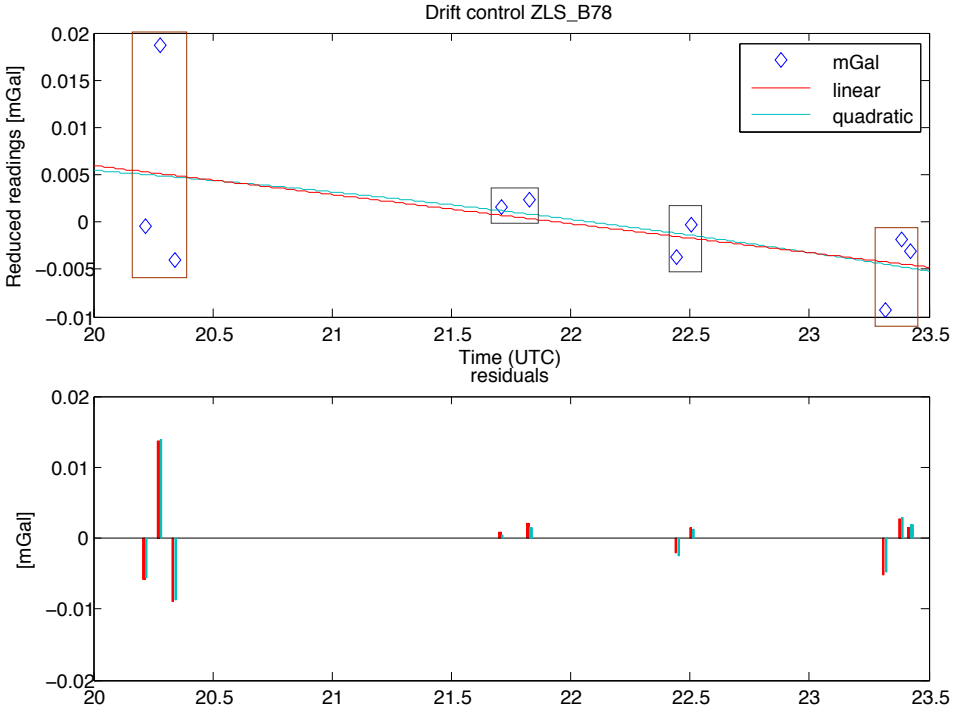

Figure 4.12: Reduced gravity readings by ZLS B-78 for the time period 20:00 to 23:40. Gravity stations: G09-2 and G13

Adjustment computations

In preprocessing, the relative gravity measurements the values were reduced for Earth tide and the height differences between the instruments and the bolt (instrument height) placed in the tunnel wall at each station. The instrument height was multiplied with the local gravity gradient measured at gravity station AG_01 to get the values referenced to a fixed position.

Adjustments of the observations were conducted with a least square method where the unknowns are calculated with

$$x = (A^T P A)^{-1} A^T P l \tag{4.7}$$

where l is the observation matrix containing all the relative gravity measurements and a pseudo observation. The design matrix A have the size [n,m] with n equal to numbers of observations and an added row for a pseudo observation, and m equal to number of gravity stations added with columns for offset and drift parameter. The values measured by LCR G-761, ZLS B-78 measurements from 10:00 to 18:00 is adjusted separate and combined.The pseudo observation is given as the absolute gravity value from processing with the merged session.

The apriori uncertainties of the relative measurements were set to 30 μGal and the weight matrix P includes these values along the diagonal. With varying precision from the relative observations, the uncertainty of the pseudo observation containing the absolute value are calculated with equation 4.4 and set to 6.6 μGal. To find the uncertainties of the relative measurements, one adjustment were performed using 0 as a pseudo observation and the uncertainty of the absolute value at 1.2 m above ground. With this, measurements at later missions can compare values in conjunction with a gravity gradient measured at that time.

The reference standard deviation *S0* expresses the quality of the model with the apriori uncertainties.

$$S0 = \sqrt{\frac{V^T P V}{(n-e)}} \tag{4.8}$$

V is the residuals of the system and calculated with

$$V = Ax - l \tag{4.9}$$

where n is the number of observations and e the number of unknown (gravity values for each station, drift and offset).

The $S0$ tells if the weights have been set too optimistic or too pessimistic, and with scaling the covariance with $S0$, a new reference standard deviation can be estimated. When $S0 \approx 1$ the uncertainties for each absolute value were calculated with the square root of the diagonal entries of the matrix P

$$\sigma = \sqrt{P_{Diagonal}} \tag{4.10}$$

The adjustments of the relative values were computed separately for the two instruments and is presented in Table 4.9.

Table 4.9: Seperately adjusted relative values for LCR G-761 and ZLS B-78

Station	LCR G-761		ZLS B-78		
G5			24.4520	± 0.0070	mGal
G09-1			16.1077	± 0.0072	mGal
G09-2			16.6546	± 0.0066	mGal
G10			13.7741	± 0.0073	mGal
G11			13.2805	± 0.0071	mGal
G12			4.9862	± 0.0067	mGal
G12-B			0.8380	± 0.0068	mGal
G13			-0.4880	± 0.0065	mGal
G14			-0.4695	± 0.0054	mGal
G15-1	0.000	± 0.0035	0.0000	± 0.0035	mGal
G15-2			-0.2137	±0.0055	mGal
G20	-4.5437	± 0.0055	-4.4626	± 0.0057	mGal
G21	-6.5052	± 0.0057	-6.4459	± 0.0056	mGal
G22	-5.5316	± 0.0063	-5.4712	± 0.0049	mGal
G23	-2.4384	± 0.0060	-2.3677	± 0.0055	mGal
G24	-4.0830	± 0.0062	-4.0342	± 0.0055	mGal
G24-B	-3.4574	± 0.0066	-3.4251	± 0.0049	mGal
G26	-1.5294	± 0.0067	-1.4557	± 0.0055	mGal
G26-B			-0.0662	± 0.0055	mGal
G27	1.5180	± 0.0070			mGal
AG_01			-0.0612	± 0.0051	mGal

The adjusted values for the combined observations is presented in Table 4.10 where pseudo observations have been added to calculate both the absolute gravity values for all the existing gravity stations, and the relative difference between the observations. The adjusted values for the combined observations from the relative instruments demonstrated higher uncertainties than expected from whatwas presented from the separate adjustments. There might be a scale difference in one of the instruments that should have been accounted for. The uncertainties have been evaluated separately to find possible deviation in the raw values.

Table 4.10: Combined adjusted absolute values for LCR G-761 and ZLS B-78

Station	Absolute values		Relative values		
G5	982227223.0	± 12.3	24513.3	± 10.9	μGal
G09-1	982218878.7	± 12.8	16169.0	± 11.5	μGal
G09-2	982219425.6	± 11.1	16715.8	± 9.5	μGal
G10	982216545.1	± 13.0	13835.3	± 11.8	μGal
G11	982216051.4	± 12.7	13341.7	± 11.3	μGal
G12	982207757.2	± 11.4	5047.4	± 9.9	μGal
G12-B	982203609.0	± 11.8	899.3	± 10.4	μGal
G13	982202282.9	± 10.9	-426.8	± 9.3	μGal
G14	982202301.4	± 10.2	-408.3	± 8.5	μGal
G15-1	982202771.0	± 10.6	61.23	± 9.0	μGal
G15-2	982202557.3	± 10.2	-152.4	± 8.5	μGal
G20	982198273.8	± 12.7	-4436.0	± 11.4	μGal
G21	982196302.5	± 12.7	-6407.2	± 11.4	μGal
G22	982197282.8	± 12.3	-5426.9	± 11.0	μGal
G23	982200377.6	± 12.7	-2332.1	± 11.4	μGal
G24	982198723.4	± 12.8	-3986.3	± 11.4	μGal
G24-B	982199344.2	± 12.4	-3365.5	± 11.1	μGal
G26	982201292.0	± 12.9	-1417.7	± 11.6	μGal
G26-B	982202692.9	± 13.9	-0016.8	± 12.7	μGal
G27	982204329.9	± 14.5	1620.1	± 13.3	μGal
AG_01	982202709.7	± 6.6	0	± 3.5	μGal

4.3 Discussion of the gravity values

The gravity gradient (Table 4.1) is used for calculations of the absolute gravity readings in the g9 software and further to lower the value from 1.2 m to the ground (0 m). With a standard deviation of ± 0.0047 μGal/m the measurements is deteriorated with ± 5.64 μGal when lowering the value to ground level. This is a higher uncertainty than what have been accomplished with the same instrument earlier in spring 2014. The gravity gradient measurements should have been repeated after dismantling the FG5 instrument to possibly obtain a smaller uncertainty, but due to lack of time, this was not conducted.

The set scatter of the absolute readings from FG5 is ± 3.47 μGal, which is of poorer precision than expected from this instrument as the manufacturer reports an instrumental accuracy of 1-2 μGal (Microg-Lacoste, 2014). Combined with the uncertainty of the gravity gradient the total uncertainty of the absolute value on ground level ends at 6.62 μGal, a value more than three times as expected. The measuring site probably had great impact, and it is hard to say if gravity station AG_01 is inclined to give measurements of higher precision. Possible reasons for the precision values can be contact between the housing and the construction form work around the pillar, making movement of persons in the house to vibrate the pillar. If persons are using the laboratory during the day, this might affect the results. However, no direct

correlations between the distinguished sets and external factors were found. With the assumption of no contact, no adjustments of the insulation layer around the pillar were made during the mission, but this should be tested at later missions.

The drift plots of the relative measurements, displayed in section 4.2.3 demonstrated linear drift trends for the separated time periods. With residuals lower than 15 μGal this correlated highly with the uncertainties of the relative values shown in Table 4.10 which all are of lower than 15 μGal. The values for the gravity stations measured with both LCR G-761 and ZLS B-78 coincided and no direct effect of the unstable battery connection of the LCR G-761 instrument was found in the uncertainties.

With the uncertainties in the combined adjusted values an offset in one or several raw values might be present, but this was not detected. The difference in the separate adjusted gravity values for stations G20 to G26 show higher deviations than the uncertainties. The error influencing these values was not found.

5 — Modelling of temporal mass variations

For identifying the factors influencing the gravity stations in the subglacial laboratory and the tunnel beneath Engabreen (Table 5.1), modelling of temporal mass variations can be done successively. Effects from glacier ice changes have been calculated for each station in order to see variations through the tunnel. Effects of masses in tunnel system have been calculated for separate stations.

Table 5.1: Coordinates of the gravity stations

Station	Latitude	Longitude	Height
G5	66° 41' 08.7576" N	13° 47' 14.9939" E	515 m
G9-1	66° 41' 01.4892" N	13° 47' 15.7227" E	532 m
G9-2	66° 41' 01.6764" N	13° 47' 15.4229" E	531 m
G10	66° 40' 54.5196" N	13° 47' 16.2320" E	547 m
G11	66° 40' 48.4860" N	13° 47' 16.0510" E	560 m
G12-1	66° 40' 39.6192" N	13° 47' 27.5017" E	584 m
G12-2	66° 40' 33.5316" N	13° 47' 34.8942" E	599 m
G13	66° 40' 29.5320" N	13° 47' 39.6921" E	609 m
G14	66° 40' 25.9860" N	13° 47' 45.2999" E	610 m
G15-1	66° 40' 25.5360" N	13° 47' 44.9347" E	610 m
G20	66° 40' 15.1716" N	13° 47' 37.4619" E	613 m
G21	66° 40' 11.4960" N	13° 47' 17.8009" E	614 m
G22	66° 40' 11.5212" N	13° 46' 46.7431" E	616 m
G23	66° 40' 14.2140" N	13° 46' 37.1091" E	618 m
G24	66° 40' 20.0640" N	13° 46' 15.8472" E	621 m
G24-B	66° 40' 22.2420" N	13° 46' 10.3295" E	622 m
G26	66° 40' 27.8400" N	13° 45' 52.4453" E	624 m
G26-B	66° 40' 28.8804" N	13° 45' 52.9963" E	626 m
G27	66° 40' 29.7516" N	13° 45' 54.6187" E	630 m
AG_01	66° 40' 25.8420" N	13° 47' 44.7503" E	609 m

5.1 Effects of glacier ice

NVE has contributed two surface models of the Engabreen drainage basin related to 2001 and 2008 (Fig. 5.1). The models have been derived from laser scanning of the surface. The model of the 2001 surface has a resolution of 5 × 5 m, while the model over the 2008 surface has a resolution of 10 × 10 m. The accuracy of surface models derived from laser scanning is principally affected by uncertainties in the laser range and GPS (Global Positioning System) position. Laser range may give uncertainties of $\sim$ 7 cm and the GPS position $\sim$ 10 cm (Kennett and Eiken, 1997).

The vertical component (eq. 3.21) of change in glacier surface was modelled with prisms of the size 5 × 5 m (see section 3.5). The lower boundary of the prism corresponded to the model surface from 2008 and the upper boundary was set to inspected height value. The density of the prism volume was here set equal to the density of glacier ice, 900 kg/m^3. Modelling of glacier surface change expected equal increase or decrease of height for the whole area. Adding or subtracting heights ± 1 m would give nearly the same results only with opposite signs and calculations were done with height difference of -1.0 m, -0.5 m, -0.1 m, -0.05 m, -0.01 m and -0.005 m from the reference surface. The resulting effects of ablated ice modelled on the surface from 2008 is presented in Table 5.3.

The main area of the glacier surface is at higher elevations compared with the gravity stations in the tunnel (see Fig. 5.2). Ice differences at higher or lower elevations affect the vertical gravity component different. In case of negative mass anomaly above the gravity stations, the gravity will increase and the mass loss will contribute with positive effects. For negative mass anomaly below the station, the mass loss will contribute with a negative effect, and the gravity will decrease. Table 5.2 display the effects in context with mass anomaly above or below calculation point.

Table 5.2: Mass anomaly effects

Mass anomaly:	Negative	Positive
Above	+	-
Below	-	+

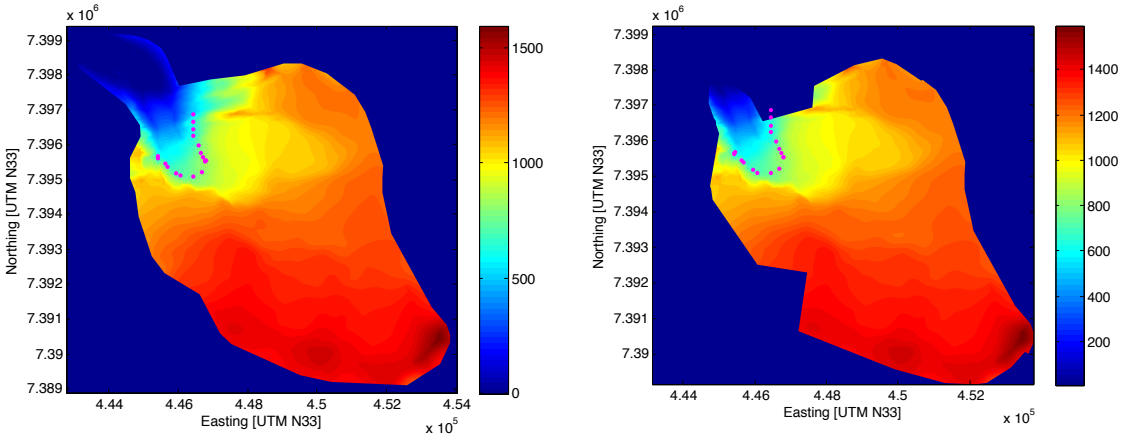

a) b)

Figure 5.1: Surface models of Engabreen drainage basin with gravity stations marked for models derived from laser scanning in a) 2001 and in b) 2008. Unit of colorbar is meter

Table 5.3: Effect of height differences on the glacier ice surface

Station	1 m	0.5 m	0.1 m	0.05 m	0.01 m	0.005 m	
G5	62.0	31.0	6.2	3.1	0.6	0.3	μGal
G09-1	146.4	73.2	14.7	7.3	1.5	0.7	μGal
G09-2	141.1	70.6	14.1	7.1	1.4	0.7	μGal
G10	315.1	157.5	31.5	15.7	3.1	1.6	μGal
G11	382.1	190.9	38.2	19.1	3.8	1.9	μGal
G12	343.6	171.8	34.3	17.2	3.4	1.7	μGal
G12-B	335.7	167.8	33.6	16.8	3.4	1.7	μGal
G13	340.0	170.0	34.0	17.0	3.4	1.7	μGal
G14	346.8	173.4	34.7	17.4	3.5	1.7	μGal
G15-1	348.0	174.0	34.8	17.4	3.5	1.7	μGal
G20	377.2	188.6	37.7	18.9	3.8	1.9	μGal
G21	397.3	198.6	39.7	19.9	4.0	2.0	μGal
G22	402.8	201.3	40.2	20.1	4.0	2.0	μGal
G23	416.5	208.1	41.6	20.8	4.2	2.1	μGal
G24	323.4	161.7	32.4	16.2	3.2	1.7	μGal
G24-B	296.0	148.1	29.6	14.8	3.0	1.5	μGal
G26	295.9	148.1	29.6	14.8	3.0	1.5	μGal
G26-B	304.0	152.0	30.4	15.2	3.0	1.5	μGal
G27	214.5	107.1	21.4	10.7	2.1	1.1	μGal
AG_01	347.2	173.6	34.7	17.4	3.5	-1.7	μGal

Effect of glacier surface change in the time period 2001 to 2008

To model the effect on the gravity stations from surface change in the time period from September 2001 to September 2008, the surface model from 2001 was subtracted

from the 2008 surface model. Comparing surface models from the same time of year precluded elevations changes due to thick layers of snow as the seasonal variations are smaller than comparisons of autumn and spring elevations. The two surface models do not cover the exact same area and restrictions on the boundaries for calculation were set to the boundaries of the 2008 model as this cover a smaller area. Comparisons of the glacier surface reveal the magnitude of surface height change in the time period of 7 years (Fig. 5.2). The effect of this change on the gravity stations was modelled with 5 × 5 m prisms and the upper and lower boundary corresponding to the surface of 2001 and the surface difference. The density was set to 900 kg/m^3. The resulting effects of surface difference between 2001 and 2008 are presented in Table 5.4.

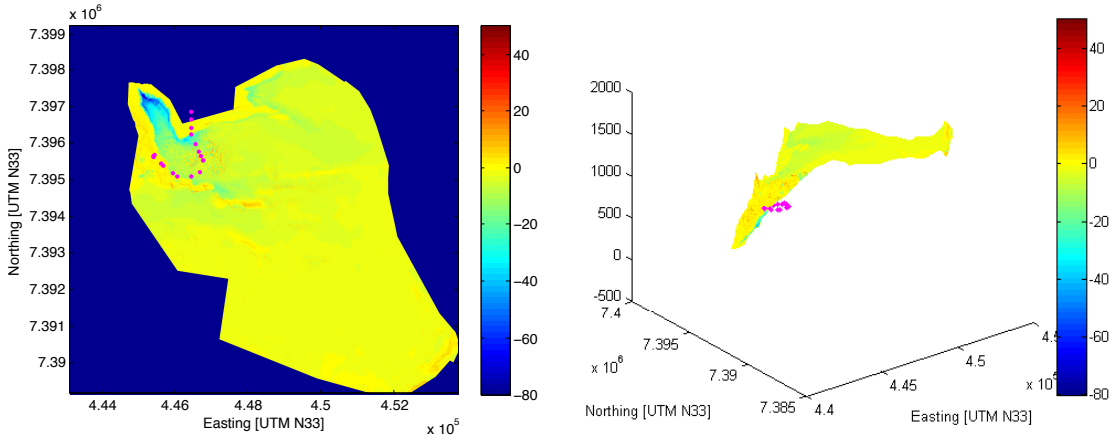

a) b)

Figure 5.2: Model of surface difference [08-01] with gravity stations marked, of models a) of whole surface and b) of whole surface displayed in 3D. Unit of colorbar is meter

Table 5.4: Effect of glacier ice surface changes between 2001 and 2008

Station		
G5	3.6	μGal
G09-1	27.7	μGal
G09-2	26.2	μGal
G10	104.1	μGal
G11	433.4	μGal
G12	332.1	μGal
G12-B	213.7	μGal
G13	182.1	μGal
G14	172.4	μGal
G15-1	172.8	μGal
G20	206.7	μGal
G21	233.6	μGal
G22	186.2	μGal
G23	200.1	μGal
G24	14.9	μGal
G24-B	-12.4	μGal
G26	-46.8	μGal
G26-B	-57.3	μGal
G27	-74.9	μGal
AG_01	172.7	μGal

5.1.1 Effect of snow cover on the glacier surface

www.senorge.no is an open internet portal with weather and climate data from three different Norwegian institutes; NVE, Kartverket and Norwegian Meteorological Institute. Together, they contributed a time series dating from 1957 with Norwegian weather conditions, divided into category's of snow, water, weather and climate. Daily maps with interpolated data from observed temperature and precipitation can be downloaded in grids with size 1000 x 1000 m for the whole country. Height differences of the snow coverage from this time series can be used to model the gravity effect in the gravity stations.

To model effect of snow cover on the gravity stations, data has been collected from grids close to the tunnel coordinates. Due to very time-consuming downloading from the weather portal, the polygon in figure 5.3 visualizes what area the data has been downloaded from. For each coordinate in the entire country, values for chosen precipitation measurements can be downloaded for time series going back to January 1st 1957. For this study, values for snow cover on April 30th, 2013 have been used. For the same area the snow cover was measured to 0 m in August 2012, which leads the values in April 2013 to reflect the total amount of snow layer for that particular season. With no knowledge of the density of the snow, modelling of the effect has been done with 100, 400 and 800 kg/m^3 and with prisms of the same size as the data set.

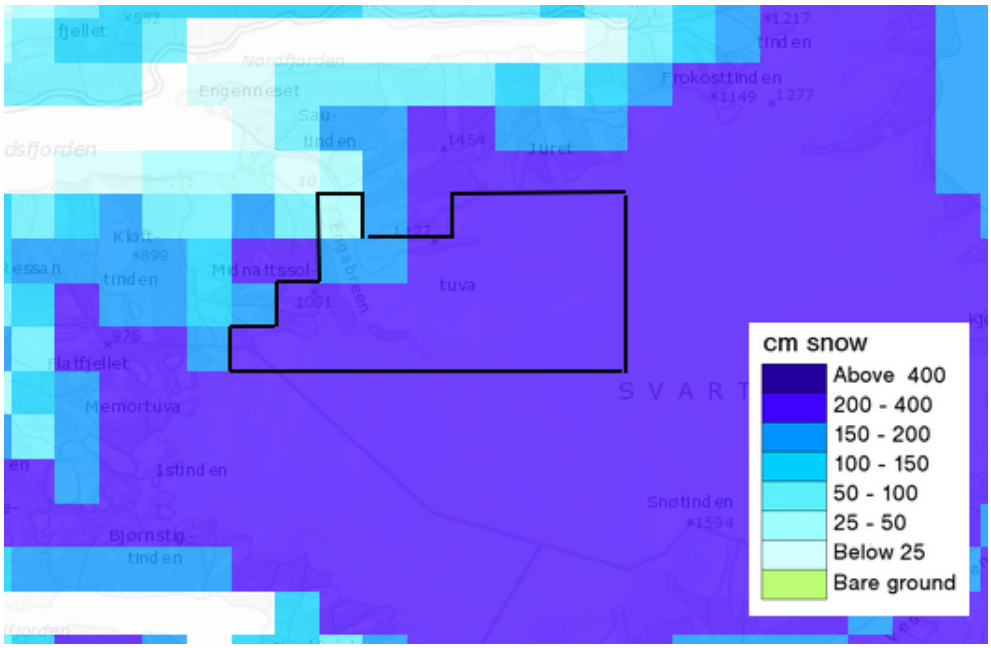

Figure 5.3: Polygon of area where data have been collected (senorge.no, 2014)

Table 5.5: Effect of snow cover on the glacier surface

Station	100 kg/m ^{3}	400 kg/m ^{3}	800 kg/m ^{3}	
G5	-0.7	-2.3	-5.8	μGal
G09-1	-0.9	-3.4	-7.0	μGal
G09-2	-0.9	-3.4	-6.9	μGal
G10	-0.9	-3.7	-7.5	μGal
G11	-1.0	-4.0	-8.1	μGal
G12	-0.9	-3.6	-7.2	μGal
G12-B	-1.0	-4.0	-7.	μGal
G13	-1.1	-4.3	-8.5	μGal
G14	-1.1	-4.5	-8.9	μGal
G15-1	-1.1	-4.5	-8.9	μGal
G20	-1.2	-4.6	-9.2	μGal
G21	-1.1	-4.4	-8.7	μGal
G22	-1.1	-4.4	-8.7	μGal
G23	-1.0	-4.0	-8.1	μGal
G24	-1.0	-3.9	-7.8	μGal
G24-B	-1.0	-3.8	-7.7	μGal
G26	-0.9	-3.6	-7.2	μGal
G26-B	-0.9	-3.5	-7.0	μGal
G27	-0.9	-3.4	-6.8	μGal
AG_01	-1.1	-4.4	-8.9	

5.1.2 Effects of sediment chamber

The tunnel system leads the melt water from the intakes to Storglomvatn reservoir. To lead as little as possible of the coarse particles from the ice and tunnel system to the reservoir, a sediment chamber was built as part of the tunnel system in the mountain (Fig. 5.4). The chamber is 140 m long and 8 m wide, large enough to still the incoming water and allow the particles to sink to the ground. During a year, the amount of sediments are measured with profiling along the length of the chamber. Annually, the sediments are flushed into a separate tunnel leading away from the water reservoir.

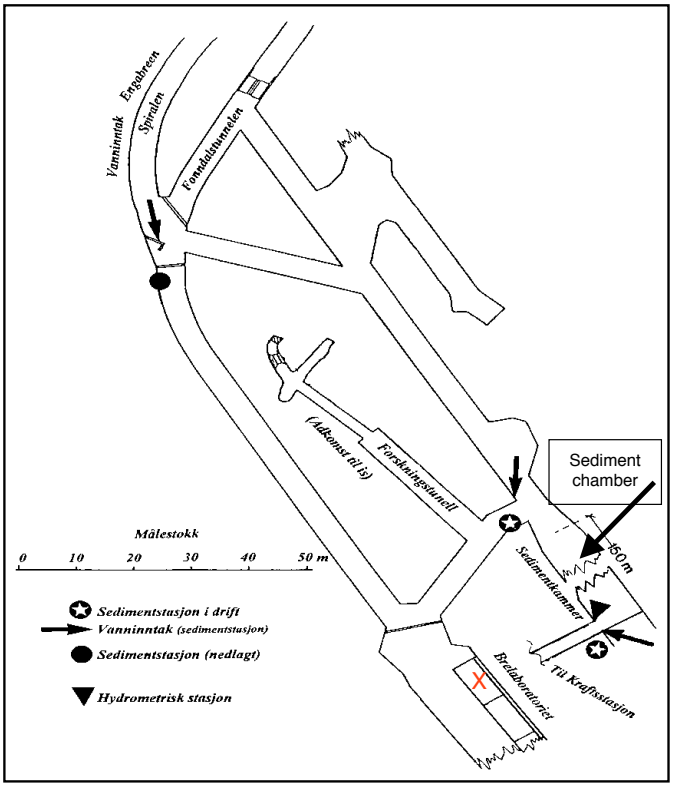

Figure 5.4: Overview of the laboratory buildings and the sediment chamber. Red cross marks gravity station AG_01 NVE (2011)

The sediment chamber is near to the gravity station AG_01 and the direction of the chamber is parallel with the tunnel to the laboratory. To control for effects from the sediments, this layer was modelled by a rectangular cubic prism. The coordinates and the geometry of the calculation were derived from the documentation file from the survey. Values of the height profile of the sediment layer after the rinsing of the chamber were collected from NVE's Oppdragsrapport 7-2102, Storglomfjordutbyggingen, page 46. A profile of the sediment depth was conducted by Miriam Jackson in March

2014. Table 5.6 and Fig. 5.5 shows the deviation between the two profiles. NVE used an estimate of vertical distance from bridge to chamber floor of 14 m for the whole chamber. This, however, was not exact measurements as the chamber floor has a slope towards the water outlet. For both data sets, the effect has been calculated with prisms covering 10 × 8 m with corresponding heights of the sediment layer of the distance from the water intake (Fig.. 5.6). The density of the sediments were set to 1600 kg/m^3 (NVE, 2011). The effects modelled from the sediment layer are presented in Table 5.7.

Table 5.6: Profile of sediment layer over chamber floor

Distance from water intake	Sediment layer in meter After rinsing	March 2014
0 m	7	8.5
10 m	5	6.7
20 m	4.5	5.3
30 m	4.5	5.1
40 m	4.0	4.5
50 m	3.5	4.4
60 m	3.2	4.0
70 m	3.0	3.5
80 m	2.8	2.5
90 m	2.2	2.6
100 m	1.5	2.2
110 m	1.2	1.2
120 m	1.0	1.2
130 m	1.0	0.5
140 m	0.0	0.0

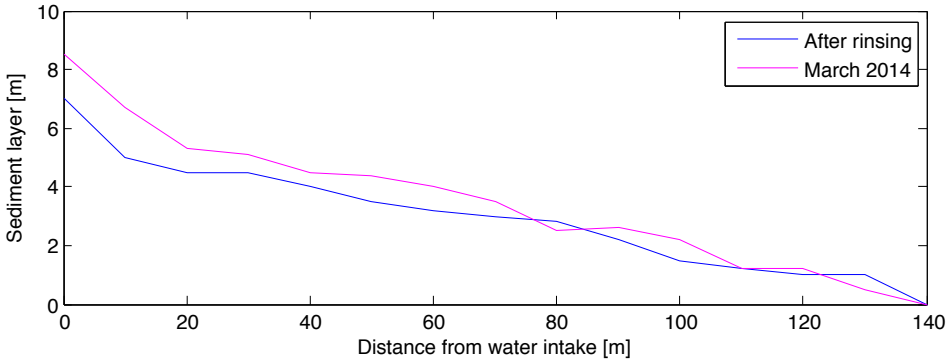

Figure 5.5: Profile of sediment layer with distance from water intake

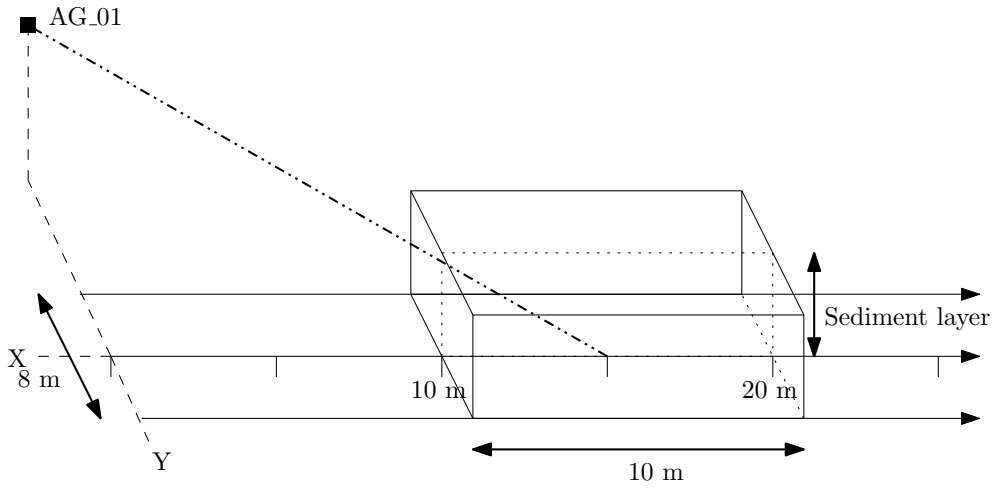

Figure 5.6: Geometry of sediment chamber, prisms and gravity station AG_01

Table 5.7: Effect of sediment layer in gravity station AG_01

Distance from water intake	Effect of sediment layer After rinsing	March 2014	
0 m	9.2	10.4	μGal
10 m	6.0	7.5	μGal
20 m	4.1	4.6	μGal
30 m	2.8	3.1	μGal
40 m	1.8	1.9	μGal
50 m	1.1	1.3	μGal
60 m	0.7	0.9	μGal
70 m	0.5	0.6	μGal
80 m	0.3	0.3	μGal
90 m	0.2	0.2	μGal
100 m	0.1	0.2	μGal
110 m	0.1	0.1	μGal
120 m	0.0	0.1	μGal
130 m	0.0	0.0	μGal
140 m	0.0	0.0	μGal
Total	26.9	31.2	μGal

5.1.3 Effects of water in the water tunnel

The effect of the water passing by each gravity station in the water tunnel was modelled by rectangular cubic prisms. With the amount of water in the water tunnel varying seasonally, the effect of the water passing each gravity station was modelled for the conditions in March 2014. To control for different effects of different prism sizes, the water volume was modelled with both one larger rectangular prism, as well as two smaller rectangular prisms covering the same volume (Fig. 5.7). The resulting effects were either 1.70 μGal using one prism and 1.13 μGal using two prisms at gravity stations G20. For comparisons of conditions in March 2014, and later missions,

figures from the gravity stations with the values from March 2014 can be found in the appendices.

The prisms are modelled with one rectangle going in a perpendicular direction to the distance measured between the gravity stations and the water depth. The resulting effects of one prism is presented in Table 5.8

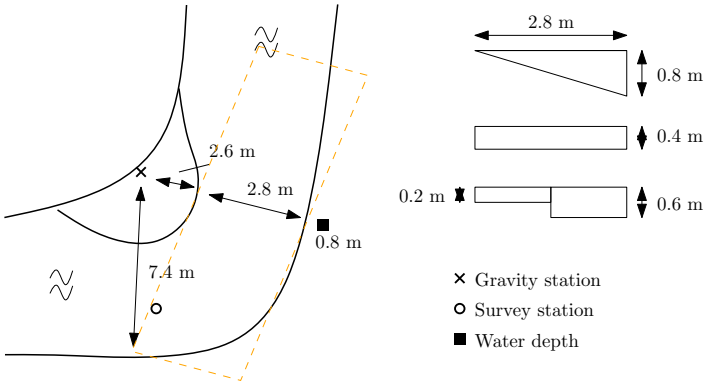

Figure 5.7: Gravity station G20

Table 5.8: Effect of water level on gravity stations in the water tunnel

Gravity station	5 m	10 m	20 m	50 m	100 m	
G20	1.2	1.7	2.0	2.1	2.1	μGal
G21	0.3	0.4	0.5	0.5	0.5	μGal
G22	0.1	0.1	0.1	0.2	0.2	μGal
G23	0.1	1.4	1.7	1.8	1.8	μGal
G24	0.5	0.5	0.5	0.5	0.5	μGal
G25	0.0	0.0	0.0	0.0	0.0	μGal
G26	1.0	1.4	1.7	1.8	1.8	μGal

6 — Investigation on glacier thickness

NVE contributed with seismic data of the topography underneath the glacier. These data make it possible to estimate the height of the glacier in each position, and the boundaries between the rock surface and the glacier can be identified. The spatial resolution of the dataset was originally 100 × 100 m, but the precision is unknown. When compared with the surface models derived from laser scanning, the height difference on the lake Engabrevatnet is 5 m between the surface models and the seismic data. The two surface models correlate at this elevation.

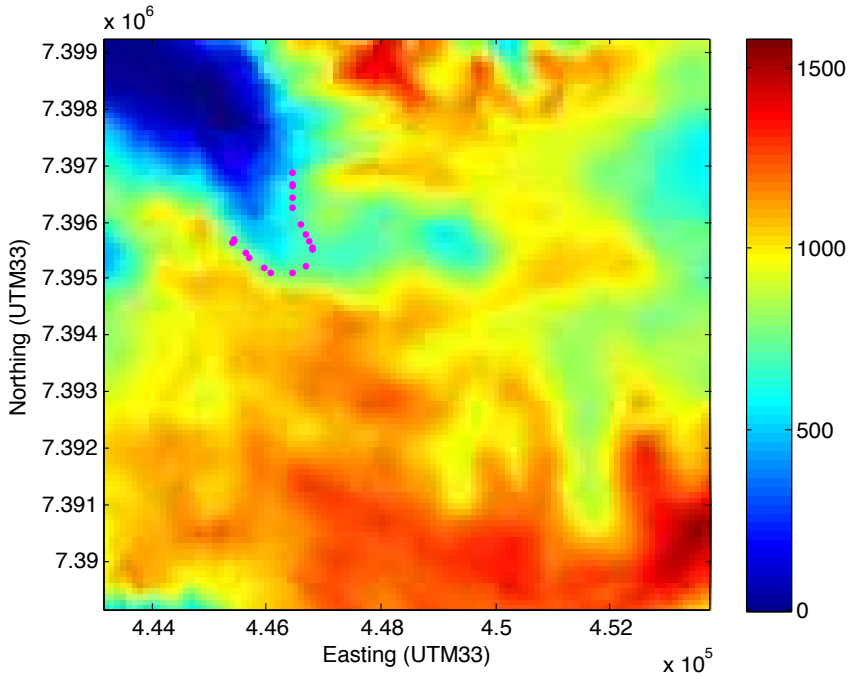

Figure 6.1: Topography model from radar scanning with gravity stations marked. Unit of colorbar is m

6.1 Effect of total glacier ice volume

The total effect of the glacier ice volume can be derived from the surface models and the topographic model from the seismic data (Figure 6.2). When modelling the effects of the total ice mass on the gravity stations, the lower boundaries of the prisms are collected from the seismic measurements and the upper boundaries are set to the surface model from 2001 and 2008 in separate calculations (Fig. 6.3). The density of the prisms is set to 900 kg/m^3, as glacier ice. The resulting effects from the total glacier heights is presented in Table 6.1

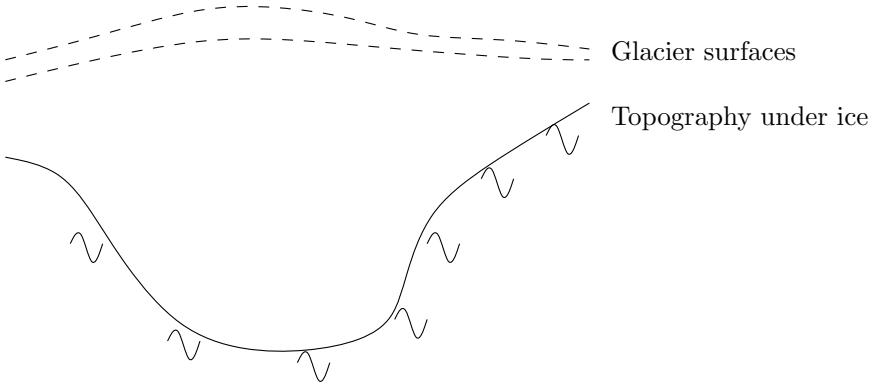

Figure 6.2: Cross section of topography under glacier ice and two glacier surfaces

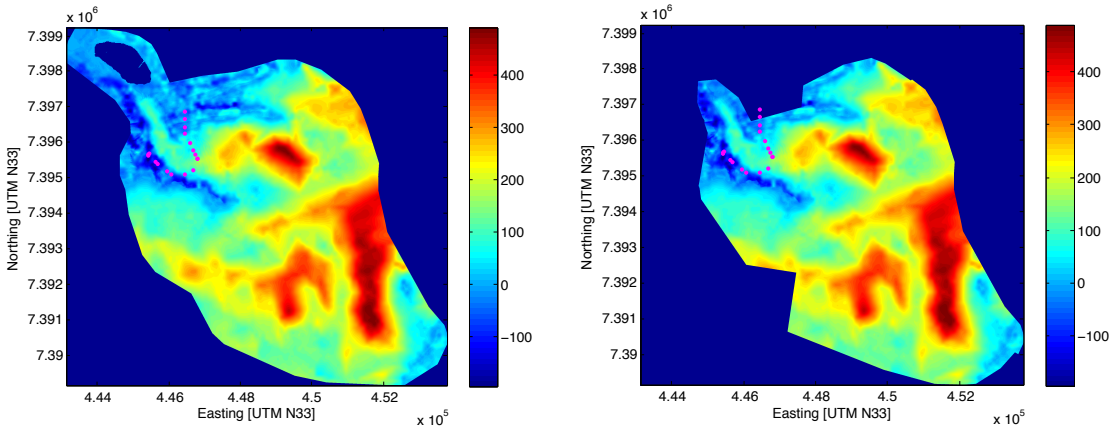

a) b)

Figure 6.3: Glacier ice height derived from bedrock topography and glacier surface with gravity stations marked using models derived from laser scanning in a) 2001 and b) in 2008. Unit of colorbar is m

Table 6.1: Effects of glacier ice volume

Station	Volume of 2001	Volume of 2008	
G5	-592.3	-588.7	μGal
G09-1	-651.2	-623.5	μGal
G09-2	-649.3	-623.1	μGal
G10	-579.8	-475.7	μGal
G11	-1295.5	-862.0	μGal
G12	-2822.5	-2490.3	μGal
G12-B	-3204.7	-2991.1	μGal
G13	-3810.4	-3628.3	μGal
G14	-4693.4	-4501.9	μGal
G15-1	-4740.5	-4567.7	μGal
G20	-3414.0	-3207.3	μGal
G21	-1728.0	-1494.4	μGal
G22	-266.0	-79.7	μGal
G23	21.3	221.4	μGal
G24	1504.3	1519.1	μGal
G24-B	1738.3	1725.9	μGal
G26	2114.4	2067.6	μGal
G26-B	2244.5	2187.2	μGal
G27	2517.9	2443.0	μGal
AG_01	-4677.7	-4505.0	μGal

6.2 Unaffected position of glacial mass change

If forthcoming missions are conducted with only relative gravimeter it is possible to establish a gravity stations at a distance from the glacier not affected by the glacier mass change, and use this as a reference gravity. Using prisms with upper and lower boundaries correlated with the surface change from 2001 to 2008, calculations can be done for a whole grid of coordinates. The density of the prisms is set to 900 kg/m^3. Figure 6.4 show the bedrock topography boundaries for the calculations and the effects on the bedrock in distance from the glacier.

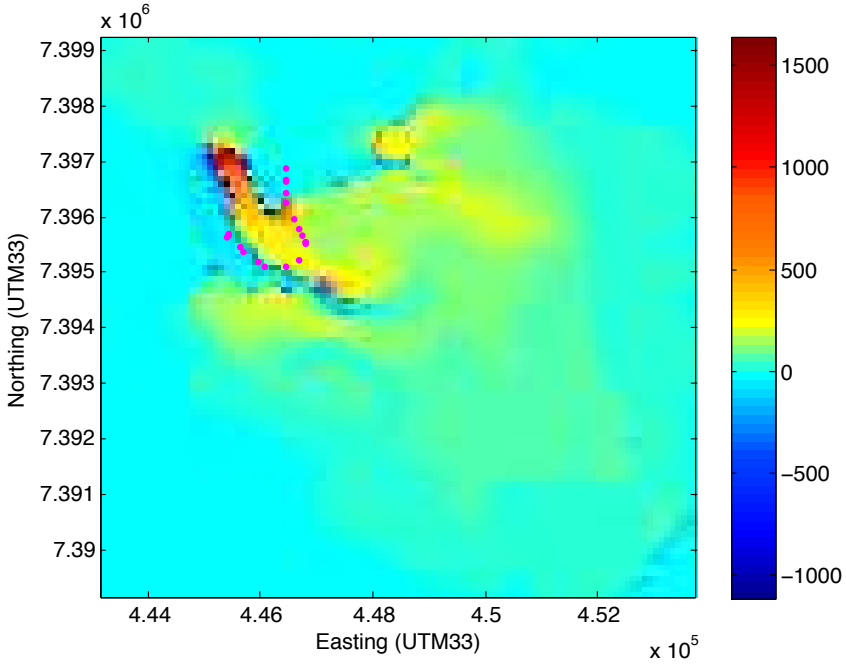

Figure 6.4: Model of vertical gravity effects of surface differences from 2001 to 2008. Unit of colorbar is μGal

Coordinates of unaffected position of glacier ice mass differences from 2001 to 2008 have been found for a position where the effect of the glacier ice mass equal to zero.

Easting:	447008.516
Northing:	7398172.076

The coordinates is presented in a map in Figure 6.5.

The unaffected coordinates should be close enough to be reached by foot forth and back from the tunnel enctrance. However, the surrounding mountains are steep and in winter time covered with snow. A more easy access can be achieved in summer time, but the water tunnel will be inaccessible due to the amount of water.

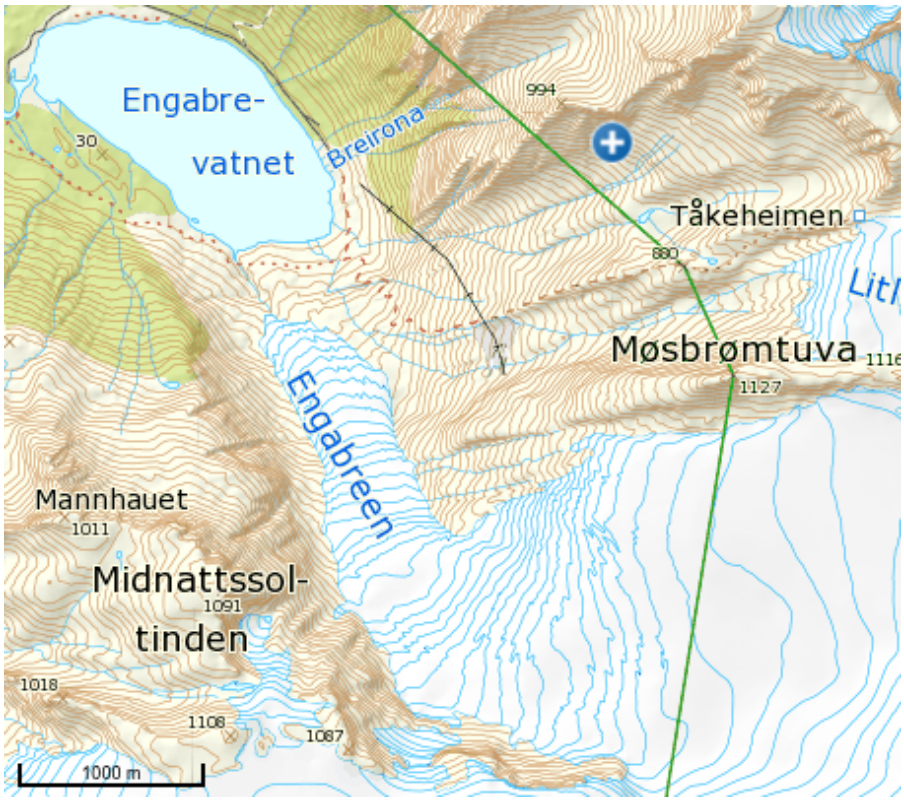

Figure 6.5: Unaffected position of glacier mass difference from 2001 to 2008

6.3 Investigation on bedrock topography precision under glacier ice

A technique for determining the thickness of glacier ice using gravity profiling was conducted by Klingele and Kahle (1977). Comparisons with seismic measurements of the glacier bed were used to define the accuracy. The gravity profile was set to be two parallel profiles cross-sectioning the length of the glacier, with two profiles local gravity disturbance, e.g. water holes in the ice, can be avoided. The elevations of the gravity stations along the profile were determined by levelling to have sufficient accuracy for reducing the gravity data. The topographic effects of the glacier surface were reduced with concentric circles divided by radial lines. The circles had radii up to 2.5 km. For distances within 20 m from the gravity stations, levelled heights were used, for distances between 20 m and 2.5 km, the height was obtained from topographic maps of the area. A Bouguer anomaly was determined with the average values from the two profiles. The observed Bouguer anomaly were compared with the regional gravity field of the area, and the residual anomaly derived from the gravity data alone differed with less than 2 mGal, which could reflect the glacier effect. To calculate the gravity effect of the glacier model, derived from seismic measurements, a contrast density of -1770 kg/m^3 (glacier ice density = 900 kg/m^3, average bedrock density = 2670 kg/m^3) was used. Deviation from the model can be explained by e.g. layers of moraine in the ice, or differences in the bedrock density, and from choice of regional gravity field.

The conclusions of Klingele and Kahle (1977) were that accuracies derived with such a technique depends on the validity of the regional gravity field and the reliability of the bedrock density. The technique is also useful for determining the glacier mass with repeated measurements over time.

When comparing the results of Klingele and Kahle (1977) with the measurements obtained during the mission in March 2014, an reverse method can theoretically be used to find the bedrock topography and thus improve the precision of the seismic measurements. Using the gravity gradient and gravity values below the glacier with high precision and the known surface of the glacier from laser scanning, the bedrock topography could be derived and compared with the existing seismic measurements. The method is not developed due to lack of time, but could give valuable knowledge for deriving the glacier ice mass.

7 — Discussion of the modelled effects

The effects of different height changes on the glacier ice surface are modelled with the assumption of linear accumulation or ablation of ice on the whole surface. This will probably not reflect the reality as the dynamics of the ice slide in horizontal directions and as warmer temperature and higher air pressure at lower elevation will affect the ice melting (section 2). With more precise data of accumulation and ice dynamics a more detailed calculation can be achieved. For both models laser scanning was conducted during the month of September, making comparisons of the two surfaces possible. An area on the southern edge of the glacier tongue shows positive surface change from 2001 to 2008 and this particular area is exposed for avalanches during winter seasons which will affect the surface model. With close proximity to gravity stations near the exit of the tunnel (gravity station 27) these masses will affect the modelled effects. It is unknown whether these masses are accumulated snow or ice, and this indicates an uncertainty in the modelled effects.

The calculated effects for height differences have positive signs. This correlates with the fact that the greater part of the glacier surface is at higher elevations than of the gravity stations, which makes a positive mass anomaly above the calculation coordinates. The modelled ablation below the gravity stations will affect with negative values. Figure 5.2 shows how the gravity stations are placed in context with the glacier surface, and the vertical distance from the surface to the gravity stations further into the mountain is longer than for the ones closer to the entrance and exit of the tunnel. The figure also show that gravity stations close to the entrance and exits have no glacier mass direct above and the vertical effects at these stations will only be components of horizontal gravity attraction.

The snow layer obtained from senorge.no is in gridsize of 1000 $\times$ 1000 m and the height values in the prism calculations are set for a whole grid which make a very rough model and give poor precision for the glacier tongue where the height differences are larger than on top of the ice cap. With a snow density of 800 kg/m^3 the snow should have similar effects on the gravity stations as an ice layer with density of 900 kg/m^3. However, the calculated effects from the snow cover are very different from the calculated effects from an ice layer difference of 1 m. With the gravity stations laying beneath the glacier tongue and consequently have large height difference in near

vicinity, modelled height with one value set for a prism of the size used here cannot provide good estimates of the snow effects.

The sediment chamber showed total effects of the size which make it necessary to take profiles of the sediment layer for forthcoming missions. With repetitions at shorter distances than 10 m more precise effects can be calculated. Since the thickest layer is in near vicinity of the gravity station AG_01, these masses have greater influences on the gravity stations than masses further away from the water intake. The effects from the sediment layer show likewise as the effects from surface differences positive values as the mass anomaly is positive above the chamber floor.

The rectangular shaped prisms are rough approaches for modelling the water flowing in the tunnel. A more correct geometry of the modelling prisms would provide more precise effects, however, the method used overestimates the effects compared with two parallel prisms. The calculated effect is of smaller value than the precision of the relative values for the affected gravity stations. The small deviations of the effect correlated with the length of the prism are also very small, indicating that water in close vicinity of the stations has greater effect than water at a distance.

The seismic measurements of the bedrock topography show elevation deviation of 5 m at Engabreen lake compared with the two surface models derived from laser scanning. The two surface models correlate at this elevation. The lake is not regulated for hydro power production or similar activities and the elevation should not change over time. There is no clear reason for this difference, and an uncertainty is thus connected to the calculated effects from the glacier mass.

For further interpretations and usage of the results, a closer cooperation with other fields of science interested in the calculations should be endeavoured.

8 — Concluding elements and outlook

In March 2014 a net of gravity stations with known coordinates were established in the tunnel associated with the subglacial laboratory beneath Engabreen glacier tongue. The stations were marked with bolts and marker paint for forthcoming missions. An absolute gravity value of 982202709.74 μGal with an uncertainty of $\pm$3.47 μGal was measured in the laboratory, and the uncertainty of the related gravity measurements was around $\pm$ 10 μGal. The absolute gravity values have uncertainties of around $\pm$ 12 μGal with $\pm$ 6.6 μGal at ground level on gravity station AG_01.

Modelled effects of glacier ice change show that with the precision of the gravity values established, a height difference on the glacier surface of 0.05 m can be detected in the tunnel system. As linear accumulation and ablation is assumed, uncertainties related to values obtained from surface models are not known, and the potential snow layer was calculated as glacier ice. With the basis of the available data further error analysis have not been conducted.

For forthcoming missions it is of high necessity to measure a gravity gradient with high precision on site where an absolute gravity value is measured. A gravity gradient measured with higher precision than obtained in the present work i.e. $\pm$ 0.03 μGal/cm will only give deterioration when lowering the absolute value to ground level of $\pm$ 3.6 μGal. A gravity gradient of this precision is obtainable and will provide absolute gravity values of higher precision throughout the gravity stations.

If a mission is conducted without an absolute gravimeter, relative gravity measurements can be referenced to a position where the glacial mass do not affect the gravity value. It will make it easier to conduct a gravity mission, since less equipment is needed. However, an absolute gravity should be measured again to establish trends in the local gravity field, not related to glacial mass change.

The presented results show detection of direct mass change in the glacier ice. As an addition to methods described in section 2.1 the present work could make valuable comparisons with more established methods. Combining in situ measurements of the density of the snow layers on the glacier surface, even better estimations of the total ice mass can be given. With a time series established at the subglacial laboratory

and the surrounding tunnel system, the measurements can, with a time perspective, give more precise data about the glacier mass. The glacier mass is of interest in many fields, both for hydro power production and for science related to climate change, and adaptable methods can be developed to serve different demands.

Bibliography

Andreassen, L., Winsvold, S., Paul, F., and Hausberg, J. (2012). Inventory of Norwegian glaciers. *NVE, Oslo*.

Benn, D. I. and Evans, D. J. (2010). *Glaciers and Glaciation*. Hodder Education.

Breili, K. (2009). *Investigations of Surface Loads of the Earth - Geomatrical Deformations and Gravity Changes*. PhD thesis, Department of Mathematical Sciences and Technology, Norwegian University of Life Sciences,vol. 2009:25, ISSN 1503-1667, ISBN 978-82-575-0892-0.

Breili, K. and Rolstad, C. (2009). Ground-Based Gravimetry for Measuring Small Spatial-scale Mass Changes on Glaciers. *Annals of Glaciology*, 50(50):141–147.

Geographiclib (2014). Geoideval. www.geographiclib.sourceforge.net/cgi-bin/GeoidEval. Accessed: 28.04.14.

Hofmann-Wellenhof, B. and Moritz, H. (2006). *Physical Geodesy*. Springer.

IAG (2014). International Association of Geodesy. www.iag-aig.org. Accessed: 15.02.14.

Kaser, G., Fountain, A., Jansson, P., et al. (2003). *A Manual for Monitoring the Mass Balance of Mountain Glaciers*. UNESCO.

Kennett, M. and Eiken, T. (1997). Airborne Measurement of Glacier Surface Elevation by Scanning Laser Altimeter. *Annals of Glaciology*, 24:293–296.

Klingele, E. and Kahle, H.-G. (1977). Gravity Profiling as a Technique for Determining the Thickness of Glacier Ice. *Pure and Applied Geophysics*, 115(4):989–998.

Liestøl, O. (2000). *Glaciology*. Unipub forlag.

Lysaker, D. I. (2011). Recent Satellite Gravity Missions and their Applications in the Geoscience. *KART OG PLAN*, 4-2011:266 – 273.

Microg-LaCoste (2012). g9 Users Manual. www.microglacoste.com.

Microg-Lacoste (2014). Micro-g LaCoste, Inc. www.microglacoste.com. Accessed: 29.05.14.

Nagy, D. (1966). The Gravitational Attraction of a Right Rectangular Prism. *Geophysics*, 31(2):362–371.

NASA (2014). Jet Propulsion Laboratory. http://www.jpl.nasa.gov. Accessed: 15.02.14.

NSIDC (2014). National Snow and Ice Data Center - Facts about glaciers. nsidc.org/cryosphere/glaciers/quickfacts.html. Accessed: 12.05.14.

NVE (2011). Storglomfjordutbyggingen, Hydrologiske underskelser 2010. Technical Report Oppdragsrapport 7, NVE, Oslo, Norge.

NVE (2014a). Engabreen. www.nve.no/en/Water/Hydrology/Glaciers/Glacier-monitoring/Mass-balance-measurements/Engabreen—/. Accessed: 27.04.14.

NVE (2014b). Svartisen subglacial observatory. www.nve.no/en/Water/Hydrology/Glaciers/Svartisen-subglacial-observatory. Accessed: 10.02.14.

NVE (2014c). Vannkraft. www.nve.no/no/Energi1/Fornybar-energi/Vannkraft/. Accessed: 12.05.14.

senorge.no (2014). senorge.no. Accessed: 11.04.14.

SNL (2014). Store Norske Leksikon - Svartisen. www.snl.no. Accessed: 27.05.14.

Timmen, L. (2010). Absolute and relative gravimetry. In *Sciences of Geodesy-I*, pages 1–48. Springer.

Torge, W. (2001). *Geodesy*. Walter de Gruyter.

UN (2014). UN Water: Thematic Factsheets. www.unwater.org/statistics/thematic-factsheets/en/. Accessed: 12.05.14.

USGS (2014). United States Geological Survey - Eqarthquake Hazard Program. www.eathquake.usgs.com. Accessed: 15.06.14.

vasskraft.no (2014). Svartisen Kraftverk. www.vasskrafta.no/svartisen/category128.html. Accessed: 12.02.14.

Wenzel, H.-G. (1997). Tide-generating Potential for the Earth. In *Tidal Phenomena*, pages 9–26. Springer.

A — Equipment

Table A.1 presents the equipment needed for establishing positions for gravity measurements.

Table A.1: Equipment used for establishing position for gravity measurement

Project	Equipment
Surveying	Tripod [6]
	Prism [6]
	Total Station (TOPCON GPT-3007)[1]
	GNSS Antenna (TOPCON PG-A1)[1]
	GNSS Antenna (TOPCON LEGANT2) [3]
	GNSS Recievers (TOPCON LEGACY E) [4]
Levelling	Level
	Level Rod
Gravimetry	FG5-226
	LC-R Relative Gravimeter
	Christian sitt

B — Documentation files

B.1 Documentation file from survey

Documentation file (Norwegian) with coordinates to all gravity stations in the tunnel.

DOKUMENTASJON UTJEVNINGSBEREGNINGER
****

ADMINISTRATIVE DATA
Oppdrag : Svartisen

GJENNOMSNITTSPARAMETRE
Geoidehøyde [m] : 0.000
Rotasjon [gon] : 0.00000
Målestokk [m/km] : 0.000
Nordlig loddavvik [gon] : 0.00000
Østlig loddavvik [gon] : 0.00000

DATUMPARAMETRE
System : EUREF89 - SONE 33
Akse / Sone : 33
Lang halvakse [m] : 6378137.000
Flattrykning [1/f]: 298.2572221010000
Tangeringsmeridian [deg]: 15.0000000000000
Skalafaktor : 0.999600
Addisjonskonst. nord [m]: 0.000
Addisjonskonst. øst [m]: 500000.000
Rotasjon [deg]: 0.000000

INSTRUMENTPARAMETRE
INSTRUMENT : 8: Topcon GTS-105N 6H5836

Std.avvik	Konstantdel	Avstandsavhengig
Retning :	0.00080 gon	0.00000 gon/km
Avstand :	0.005 m	0.002 m/km
Høydeforskjell :	0.000 m	0.020 m/km
Sentrering Grunnriss :	0.001 m	
Sentrering Høyde :	0.002 m	

Referanseverdier
Referansetrykk : 760.0 mmHg
Referansetemperatur : 15.0 C
Addisjonskonstant : -0.063 m
Målestokkfeil : 0.000 m/km

DATUM: EUREF89 - SONE 33

UTJEVNING I 3-D

TVUNGEN UTJEVNING

GITTE KOORDINATER [meter]

PUNKT	N	E	H
GPS2	7396965.172	446324.494	476.454
GPS3	7396913.690	446425.373	511.160
GPS4	7396910.574	446427.678	511.728
GPS29	7395688.426	445468.678	635.470

NYBESTEMTE KOORDINATER MED MIDLERE FEIL [meter]

PUNKT	N	E	H	a	sP	sH
5	7396870.989	446455.050	514.703	0.044	0.046	0.019
6	7396866.482	446458.504	515.240	0.041	0.044	0.018
7	7396849.176	446462.813	516.744	0.053	0.057	0.023
8	7396831.961	446462.906	518.038	0.059	0.064	0.026
9	7396644.964	446462.902	531.265	0.076	0.099	0.042
10	7396429.694	446461.498	546.282	0.133	0.152	0.057
11	7396242.800	446464.347	560.126	0.180	0.197	0.066
12	7395966.554	446591.375	582.984	0.248	0.268	0.091
13	7395659.436	446731.998	608.050	0.328	0.344	0.099
13S	7395644.788	446701.536	608.357	0.335	0.352	0.103
14	7395536.816	446794.250	609.312	0.362	0.380	0.102
15	7395519.607	446801.398	611.975	0.367	0.385	0.102
16	7395520.008	446805.750	612.000	0.363	0.381	0.102
17	7395441.335	446840.821	612.267	0.356	0.381	0.105
18	7395430.107	446837.049	612.076	0.355	0.380	0.105
19	7395398.732	446819.592	614.300	0.352	0.377	0.105
20	7395199.385	446695.129	613.221	0.340	0.364	0.110
21	7395090.798	446442.029	614.616	0.338	0.364	0.113
22	7395103.792	446066.482	616.640	0.335	0.365	0.108
23	7395198.787	445952.429	618.313	0.321	0.349	0.105
24	7395214.888	445875.241	618.704	0.304	0.330	0.103
25	7395577.726	445471.147	623.782	0.143	0.162	0.058
26	7395631.672	445410.103	624.554	0.119	0.143	0.050
27	7395689.670	445445.753	631.126	0.106	0.112	0.041
28	7395688.995	445461.233	630.651	0.087	0.089	0.034
17-E	7395439.619	446840.987	612.366	0.354	0.379	0.105
24-B	7395437.599	445630.196	622.000	0.191	0.219	0.077
AG-01	7395535.547	446792.502	609.517	0.374	0.395	0.110
G5	7396871.251	446453.156	514.992	0.055	0.059	0.030
G10	7396430.182	446459.778	546.751	0.158	0.175	0.066
G11	7396243.407	446453.927	560.327	0.199	0.216	0.074

G13	7395651.008	446732.636	608.778	0.331	0.357	0.105
G14	7395539.867	446799.333	610.269	0.371	0.390	0.107
G20	7395206.935	446696.672	612.694	0.345	0.375	0.116
G21	7395097.848	446453.154	613.854	0.350	0.375	0.118
G22	7395106.031	446071.968	616.050	0.346	0.376	0.113
G23	7395191.732	445955.355	618.044	0.323	0.361	0.110
G24	7395377.957	445697.966	620.559	0.239	0.283	0.136
G26	7395624.353	445415.527	624.329	0.141	0.168	0.060
G27	7395683.053	445443.371	630.141	0.113	0.143	0.053
G24-B	7395446.733	445631.577	621.834	0.193	0.234	0.084
G26-B	7395656.377	445422.926	625.696	0.129	0.163	0.061
G9-1	7396646.104	446457.723	531.915	0.115	0.133	0.054
G9-2	7396651.897	446454.292	530.828	0.115	0.132	0.054
G12-1	7395966.136	446589.093	583.656	0.263	0.282	0.097
G12-2	7395775.898	446676.153	599.433	0.305	0.334	0.121
G15-1	7395526.004	446794.581	609.743	0.368	0.393	0.108
GPS1	7397241.655	446453.817	533.195	0.057	0.069	0.047
INN	7395536.263	446790.572	610.562	0.367	0.385	0.105
S1	7395629.937	446710.214	609.336	0.341	0.367	0.108
S2	7395625.340	446712.440	609.462	0.342	0.368	0.108
S3	7395620.966	446714.755	609.473	0.344	0.370	0.109
S4	7395616.598	446717.016	609.491	0.345	0.371	0.109
S5	7395608.436	446720.999	609.537	0.348	0.374	0.109
S6	7395599.749	446725.548	609.575	0.351	0.377	0.110
S7	7395592.052	446729.647	609.599	0.355	0.380	0.110
S8	7395548.078	446752.134	609.276	0.374	0.399	0.114
S9	7395501.485	446775.859	609.386	0.399	0.423	0.121

STATISTIKK

```
Antall iterasjoner                        :           1

Antall observasjoner retning              :         120
Antall observasjoner avstand              :         120
Antall observasjoner høydeforskjell       :         120
Antall observasjoner                      :         360

Antall ukjente grunnrisskoordinater       :         116
Antall ukjente høydekoordinater           :          58
Antall ukjente orienteringselementer      :          31
Antall ukjente                            :         205

Antall overbestemmelser                   :         155

Feilkvadratsum                            :       44788.48877705
Beregnet std.avvik på vektsenheten              16.9988
Antatt   std.avvik på vektsenheten        :           1.0000
```

TEST AV M0

```
Tabellverdi    =    185.06 (Kjikvadrat, f=155, alfa=0.0500)
Beregnet verdi =  44788.49 ***
```

B.2 Documentation file from g9 processing

Documentation file from processing of both FG5 sessions merged, with all drops included.

```
Micro-g LaCoste g Processing Report
File Created: 05/25/14, 12:57:02

Project Name: Svartisen-AG-01-merge_all
g Acquisition Version: 9.120422
g Processing Version: 9.120423

Company/Institution:
Operator: SE, AH, VO

Station Data
Name: Svartisen
Site Code: AG-01
Lat:  66.67400 Long:   13.79600 Elev:  609.52 m
Setup Height: 13.12 cm
Transfer Height:  0.00 cm
Actual Height: 129.52 cm
Gradient: -2.400 µGal/cm
Nominal Air Pressure:  942.14 mBar
Barometric Admittance Factor:  0.30
Polar Motion Coord: 0.0274 " 0.4071 "
Earth Tide (ETGTAB) Selected
Potential Filename: C:\gData\gWavefiles\ETCPOT.dat
Delta Factor Filename: C:\gData\OceanLoad-Svartisen.dff
Delta Factors
     Start   Stop     Amplitude    Phase Term
  0.000000  0.000001   1.000000   0.0000 DC
  0.000002  0.249951   1.160000   0.0000 Long
  0.721500  0.906315   1.154250   0.0000 Q1
  0.921941  0.974188   1.154240   0.0000 O1
  0.989049  0.998028   1.149150   0.0000 P1
  0.999853  1.216397   1.134890   0.0000 K1
  1.719381  1.906462   1.161720   0.0000 N2
  1.923766  1.976926   1.161720   0.0000 M2
  1.991787  2.002885   1.161720   0.0000 S2
  2.003032  2.182843   1.161720   0.0000 K2
  2.753244  3.081254   1.07338    0.0000 M3
  3.791964  3.937897   1.03900    0.0000 M4
Ocean Load ON, Filename: C:\gData\OceanLoad-Svartisen.olf
Waves:               M2    S2     K1     O1     N2     P1     K2
Q1     Mf     Mm     Ssa
Amplitude (µGal):  2.946  0.999  0.577  0.402  0.673  0.188  0.234
0.150  0.000  0.000  0.000
Phase (deg):      -180.1  139.5  -15.2  123.3 -162.2  -13.1  132.9
-189.8    0.0    0.0    0.0

Instrument Data
Meter Type: FG5
Meter S/N: 226
Factory Height: 116.40 cm
Rubidium Frequency:  10000000.00860 Hz
Laser: WEO100 (202)
ID: 632.99117754 nm ( -0.41 V)
IE: 632.99119473 nm ( -0.94 V)
IF: 632.99121259 nm ( -1.37 V)
IG: 632.99123023 nm ( -1.78 V)
IH: 632.99136890 nm ( -2.14 V)
II: 632.99139822 nm ( -1.76 V)
IJ: 632.99142704 nm ( -1.37 V)
Modulation Frequency:  8333.330 Hz

Processing Results
Date: 03/21/14
Time: 09:38:44
DOY: 080
Year: 2014
Time Offset (D h:m:s): 0 0:0:0
Gravity:   982202709.74 µGal
Set Scatter:  3.47 µGal
Measurement Precision:  0.41 µGal
Total Uncertainty:  4.33 µGal
Number of Sets Collected:   72
Number of Sets Processed:   72
Set #s Processed:
1,2,3,4,5,6,7,8,9,10,11,12,13,14,15,16,17,18,19,20,21,22,23,24,25,26
,
27,28,29,30,31,32,33,34,35,36,37,38,39,40,41,42,43,44,45,46,47,48,49
,
50,51,52,53,54,55,56,57,58,59,60,61,62,63,64,65,66,67,68,69,70,71,72
Number of Sets NOT Processed:    0
Set #s NOT Processed:
Number of Drops/Set:   50
Total Drops Accepted:    3576
Total Drops Rejected:      24
Total Fringes Acquired:     700
Fringe Start:   19
Processed Fringes:    331
GuideCard Multiplex:    4
GuideCard Scale Factor:    250

Acquisition Settings
Set Interval: 60 min
Drop Interval: 10 sec
Number of Sets: 72
Number of Drops: 50

Gravity Corrections
Earth Tide (ETGTAB): -53.13 µGal
Ocean Load: -0.00 µGal
Polar Motion:  0.98 µGal
Barometric Pressure: -8.70 µGal
Transfer Height: 310.85 µGal
Reference Xo: -0.00 µGal

Uncertainties
Sigma Reject:  3.00
Earth Tide Factor: 0.001
Average Earth Tide Uncertainty:  0.05 µGal
```

```
Ocean Load Factor:  0.10
Average Ocean Load Uncertainty:  0.00 µGal
Barometric:  1.00 µGal
Polar Motion:  0.05 µGal
Laser:  0.05 µGal
Clock:  0.50 µGal
System Type:  1.10 µGal
Tidal Swell:  0.00 µGal
Water Table:  0.00 µGal
Unmodeled:  0.00 µGal
System Setup:  1.00 µGal
Gradient: 3.886 µGal (0.030 µGal/cm)


Comments
Comments:

Bullseye mot nord.




Files Merged:

Svartisen-AG-01-20140319a.fg5

Svartisen-AG-01-20140322a.fg5
```

C — Raw values from relative gravimeter measurements

korriger instr
menthgder

Table C.1: Raw values from LC-R g-761

Running index	Station number	Time (hh:mm)	Time (decimal hour)	Instrument height (m)	Counter units	Feedback (mGal)
1	G15,1	11,51	11,85	0,206	5766	-12,505
2		11,55	11,92	0,206	5766	-12,512
3	G 20	12,46	12,77	-0,247	5766	-16,96
4		12,50	12,83	-0,247	5766	-16,95
5	G21	13,12	13,2	-0,343	5766	-18,897
6		13,16	13,27	-0,343	5766	-18,9
7	G22	13,35	13,58	-0,340	5766	-17,932
8		13,38	13,63	-0,340	5766	-17,926
9	G23	13,58	13,97	-0,370	5766	-14,837
10		14,02	14,33	-0,370	5766	-14,831
11	G24	14,31	14,52	-0,593	5766	-16,43
12		14,35	14,58	-0,593	5766	-16,426
13	G24B	14,59	14,98	-0,291	5766	-15,881
14		15,03	15,05	-0,291	5766	-15,8745
15	G26	15,24	15,4	-0,442	5766	-13,913
16		15,27	15,45	-0,442	5766	-13,916
17	G27	15,42	15,7	-0,165	5766	-10,935
18		15,47	15,78	-0,165	5766	-10,933
19	G24,B	16,29	16,48	-0,292	5766	-15,879
20		16,33	16,55	-0,292	5766	-15,876
21	G22	17,00	17	-0,338	5766	-17,943
22		17,05	17,08	-0,338	5766	-17,935

Table C.2: Raw values from ZLS B78

Run. index	Station number	Time (hh:mm:ss)	Readings (mGal)	Sigma (mGal)	Instrument height (m)	Counter Units	Beam error
1	G15-1	10:50:17	5735.535	0.0405	0.235	5800.000	0.000
2	G15-1	10:54:10	5735.540	0.0227	0.235	5800.000	-0.001
3	G20	11:46:34	5731.182	0.0276	-0.181	5800.000	0.000
4	G20	11:51:02	5731.180	0.0069	-0.181	5800.000	-0.001
5	G21	12:10:13	5729.222	0.0183	-0.284	5800.000	0.000
6	G21	12:15:05	5729.226	0.0104	-0.284	5800.000	0.000
7	G22	12:37:07	5730.197	0.0099	-0.253	5800.000	0.000
8	G22	12:41:13	5730.200	0.0259	-0.253	5800.000	0.000
9	G23	13:01:10	5733.314	0.0376	-0.313	5800.000	0.002
10	G23	13:08:00	5733.312	0.0374	-0.313	5800.000	0.000
11	G24	13:35:04	5731.705	0.0083	-0.552	5800.000	-0.002
12	G24	13:38:50	5731.707	0.0161	-0.552	5800.000	0.000
13	G24-B	14:00:36	5732.243	0.0066	-0.251	5800.000	-0.003
14	G24-B	14:05:07	5732.251	0.0150	-0.251	5800.000	-0.004
15	G26	14:28:39	5734.246	0.0514	-0.382	5800.000	-0.002
16	G26	14:32:12	5734.249	0.0028	-0.381	5800.000	0.002
17	G26-B	14:47:27	5735.594	0.0297	-0.209	5800.000	0.001
18	G26-B	14:51:52	5735.600	0.0312	-0.209	5800.000	0.000
19	G24-B	15:29:25	5732.242	0.0572	-0.236	5800.000	-0.003
20	G24-B	15:34:18	5732.249	0.0256	-0.236	5800.000	0.000
21	G22	16:01:14	5730.206	0.0114	-0.269	5800.000	0.002
22	G22	16:04:44	5730.206	0.0165	-0.269	5800.000	0.000
23	G15-1	17:12:48	5735.568	0.0088	0.232	5800.000	-0.001
24	G15-1	17:17:13	5735.571	0.0065	0.232	5800.000	0.000
25	G15-1	18:15:13	5735.554	0.0260	0.234	5800.000	0.001
26	AG01	18:25:37	5735.494	0.0033	0.238	5800.000	0.000
27	G15-1	18:34:33	5735.564	0.0142	0.233	5800.000	0.000
28	AG01	18:46:36	5735.513	0.0090	0.239	5800.000	0.000
29	G14	19:01:03	5735.264	0.0162	-0.460	5800.000	0.000
30	G15-2	19:09:05	5735.456	0.0310	-0.194	5800.000	0.000

Run. index	Station number	Time (hh:mm:ss)	Readings (mGal)	Sigma (mGal)	Instrument height (m)	Counter Units	Beam error
31	G14	19:17:18	5735.267	0.0191	-0.456	5800.000	0.002
32	G15-2	19:24:42	5735.465	0.0231	-0.197	5800.000	0.000
33	G14	19:31:09	5735.273	0.0380	-0.462	5800.000	0.003
34	AG01	19:38:12	5735.518	0.0234	0.237	5800.000	0.002
35	G15-1	19:44:48	5735.580	0.0270	0.233	5800.000	-0.001
36	G15-2	19:50:36	5735.468	0.0275	-0.194	5800.000	0.001
37	AG01	19:55:55	5735.514	0.0043	0.239	5800.000	0.003
38	AG01	19:59:38	5735.511	0.0412	0.239	5800.000	-0.002
39	G13	20:13:02	5735.025	0.0226	0.000	5800.000	0.000
40	G13	20:16:44	5735.044	0.0257	0.000	5800.000	-0.001
41	G13	20:20:22	5735.021	0.0070	0.000	5800.000	-0.002
42	G12	20:33:40	5740.558	0.0216	-0.231	5800.000	-0.002
43	G12	20:38:29	5740.562	0.0338	0.231	5800.000	0.000
44	G11	20:51:43	5748.828	0.0378	-0.161	5800.000	-0.002
45	G11	20:56:17	5748.836	0.0122	-0.161	5800.000	0.000
46	G11	21:00:29	5748.835	0.0374	-0.161	5800.000	-0.001
47	G10	21:13:47	5749.310	0.0361	-0.072	5800.000	0.001
48	G10	21:17:14	5749.309	0.0301	-0.072	5800.000	0.000
49	G09-1	21:29:20	5751.688	0.0080	-0.293	5800.000	0.000
50	G09-1	21:33:32	5751.686	0.0204	-0.293	5800.000	0.000
51	G09-2	21:42:32	5752.103	0.0158	0.242	5800.000	0.002
52	G09-2	21:49:36	5752.103	0.0259	0.242	5800.000	0.000
53	G05	22:04:56	5759.976	0.0302	-0.089	5800.000	0.003
54	G05	22:14:16	5759.978	0.0297	-0.089	5800.000	-0.002
55	G09-2	22:26:43	5752.096	0.0252	0.245	5800.000	-0.001
56	G09-2	22:30:28	5752.099	0.0279	0.245	5800.000	-0.001
57	G12	22:50:13	5740.542	0.0129	-0.265	5800.000	-0.003
58	G12	22:54:58	5740.550	0.0128	-0.265	5800.000	0.000
59	G12-B	23:06:55	5736.422	0.0425	-0.368	5800.000	0.001
60	G12-B	23:11:13	5736.423	0.0467	-0.368	5800.000	0.002
61	G13	23:18:57	5735.010	0.0049	-0.033	5800.000	0.001
62	G13	23:23:08	5735.018	0.0187	-0.033	5800.000	-0.001
63	G13	23:25:23	5735.016	0.0029	-0.033	5800.000	-0.001
64	AG01	23:34:49	5735.488	0.0143	-0.237	5800.000	0.001
65	AG01	23:38:29	5735.487	0.0180	-0.237	5800.000	-0.002
66	AG01	23:40:05	5735.489	0.0034	-0.237	5800.000	-0.001

Table C.3: Gravity gradient measurements, LC-R g-761

Running index	Lower level Time (hh:mm)	g-Reading (mGal)	Upper level Time (hh:mm)	g-Reading (mGal)	g (mGal)	h (m)	g/h (mGal/m)
1	19.15	-12,486	19.18	-12,820	0,334	1,400	0,239
2	19.21	-12,490	19.25	-12,813	0,323	1,400	0,282
3	19.28	-12,490	19.31	-12,818	0,339	1,400	0,243
4	19.33	-12,490	19.37	-12,854	0,342	1,400	0,245
5	19.40	-12,490	19.37	-12,772	0,267	1,400	0,191
6	19.49	-12,490	19.52	-12,789	0,323	1,400	0,231
7	19.55	-12,490	19.58	-12,796	0,340	1,400	0,243
8	20.01	-12,471	20.04	-12,794	0,323	1,400	0,231
9	20.08	-12,471	20.11	-12,785	0,332	1,400	0,238
10	20.14	-12,471	20.17	-12,800	0,344	1,400	0,246
11	20.21	-12,471	20.24	-12,782	0,323	1,400	0,231

D — Figures of gravity stations in water tunnel

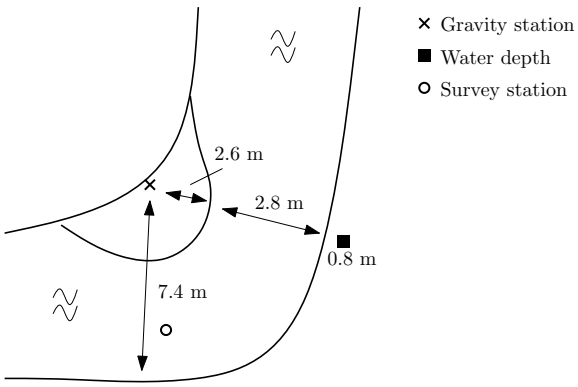

Figure D.1: Gravity station G20

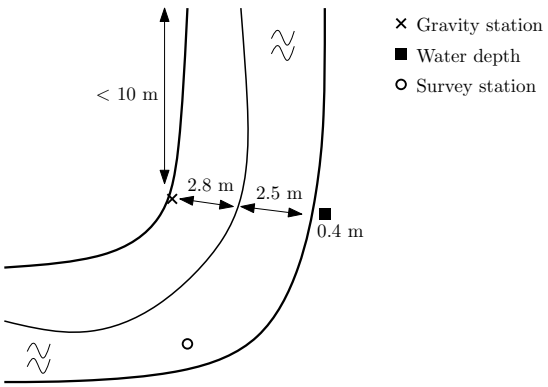

Figure D.2: Gravity station G21

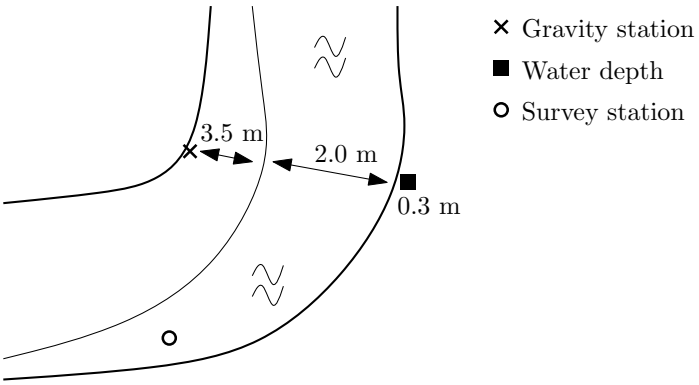

Figure D.3: Gravity station G22

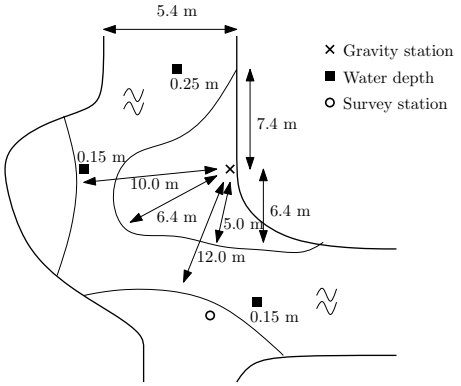

Figure D.4: Gravity station G23

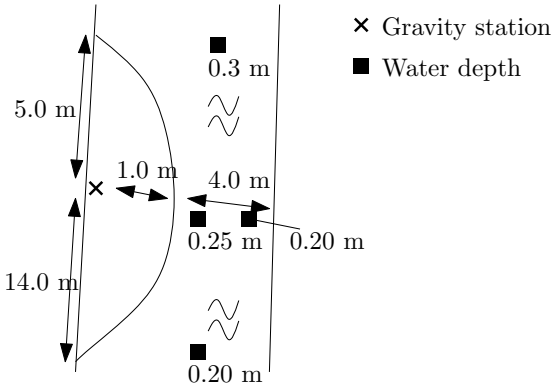

Figure D.5: Gravity station G24

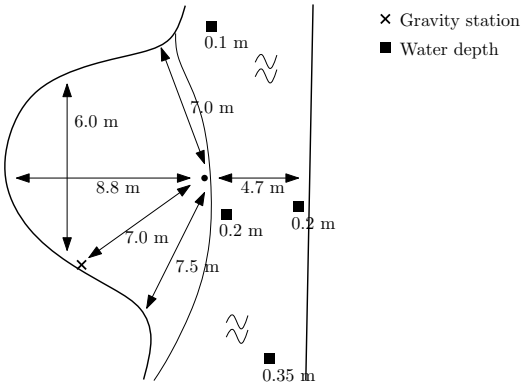

Figure D.6: Gravity station G24B

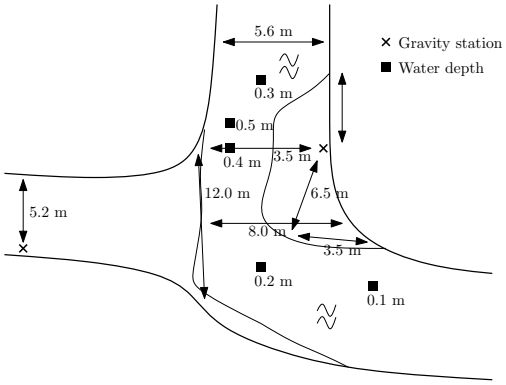

Figure D.7: Gravity station G26

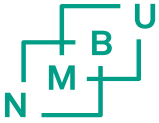

Norwegian University
of Life Sciences

Postboks 5003
NO-1432 Ås, Norway
+47 67 23 00 00
www.nmbu.no